Oligocene – Miocene Tectono-Stratigraphic Development of the Southern Levant Basin, Eastern Mediterranean

Amir Joffe [1*], Rebecca E. Bell[1], Josh Steinberg, Christopher A-L. Jackson[1,2], Yizhaq Makovsky[3]

1. Landscapes and Basins Research Group (LBRG), Department of Earth Science and Engineering, Imperial College London, South Kensington Campus, SW7 2BP, UK
2. WSP UK Ltd, Manchester, M15 4GU, UK
3. The Dr. Moses Strauss Department of Marine Geoscience and Hatter Department of Marine Technologies, Charney School of Marine Sciences, University of Haifa, 3103301 Haifa, Israel

*Corresponding author: amir.joffe18@imperial.ac.uk

Acknowledgments

We would like to thank Ratio Energies for their financial support of Amir Joffe's PhD and for providing the 2D surveys, and the Leviathan, Royee, Sara-Myra-Arie 3D seismic reflection data. We thank Ratio Energies, NewMed Energy and Chevron for approving access to the Leviathan 3D survey and the publication of this manuscript. We thank the Petroleum Commissioner in Israel Ministry of Energy for providing access to the NBL 3D survey. We would like to thank SLB for sponsoring Petrel software and Geoteric for their academic licenses for Imperial College. Kul Karcz, Omri Shitrit, Adar Glazer are thanked for fruitful discussion and support during the preparations of this manuscript.

Data Availability Statement

The data is not publicly available due to confidentiality agreements.

1. Abstract

The Levant Basin, Eastern Mediterranean, has a complex geological history. The separation of Africa from Arabia, and the collision of the latter with Eurasia during the Oligocene – Miocene had significant implications for the tectono-stratigraphy of the region, as recorded in the thick, siliciclastic-dominated sequence preserved in the Levant Basin. Previous studies mostly focused on either onshore or relatively local offshore areas, with a synthesis of the interplay between plate motions and sedimentation, as largely documented in offshore geophysical and geological (i.e., borehole) data still lacking. Using multiple high-resolution, 3D seismic reflection surveys, we generated sediment thickness maps, spectral decomposition, and ISO-proportional slices that document the structural and sedimentological elements shaping the basin during the Oligocene – Miocene. More specifically, our results show that during the Early Oligocene, sedimentation was dominated by an easterly (Arabian) source, whereas the Late Oligocene to Aquitanian witnessed a shift to a southerly (African) source through the evolution of the Nile River. The Burdigalian period marked a significant tectono-stratigraphic transition period during which large-scale folding, regional faulting and renewed incision occurred. Widespread carbonate deposition during the Langhian-Serravallian was followed, during the Early Tortonian, by a catastrophic event that mostly affected the southern Levant Basin. The Late Tortonian was largely characterised by widespread submarine incision across the southern Levant Basin. Our study reveals how sedimentary systems record important clues as to complex tectonic reorganisations involving rifting, subduction, and strike-slip motion.

2. Introduction

Sedimentary sequences capture the evolution of sedimentary basins by recording local and regional, tectono-stratigraphic events. The exposure of submerged rocks to denudation, alongside subsidence which creates space and accommodated for this material to be deposited and preserved. Whereas these regional geodynamic events influence basin subsidence, uplift, erosion, and basin-scale sediment routing, local events such as salt diapirism, and autogenic switching between channels, etc., affect intra-basin sediment dispersal (Stow et al., 1985; Bouma, 2005; Jackson et al., 2008; Howlett et al., 2021; Tillmans et al., 2021). Many studies focus on either the source (exposed rocks), the sink (submerged basins), or the sediment routing connecting the two, despite them all being genetically linked. There are significant difficulties in building a complete story connecting these three elements, due to the often-vast areal extent and multiple data sources connecting both the exposed and unexposed regions.

One area where the genetic link between onshore tectonism, sediment routing, and submerged basins is undertested is the geo-dynamically complex Levant Basin, in the Eastern Mediterranean Sea. The complexity of the Levant Basin during the Oligocene – Miocene is manifested by interaction of the African, Arabian and Eurasian tectonic plates. Arabia's separation from Africa and its collision with Eurasia triggered multiple tectonic events throughout the region. In response to these tectonic events, areas became exposed for denudation, whereas others subsided, therefore triggering new, vast rivers, such as the Nile River, all flowing towards the Levant Basin. A plethora of studies have focused on the onshore areas, describing in detail the vertical motions, and the sedimentary responses. On the other hand, there is limited knowledge published offshore, especially large-scale 3D seismic reflection data-based studies, making the offshore area, and its connection to the tectonic events recognised onshore poorly understood.

The observations presented here will demonstrate that as complex as it may be, the Levant Basin (Figure 1) is a showcase for basin-analysis, with interaction between onshore tectonics, denudation, initiation of sediment supply, and preservation of these rocks in a submerged basin. In this paper we use several new offshore 3D seismic reflection surveys to determine the Oligo–Miocene evolution of the deep-water sedimentary system in the Southern Levant Basin. By characterising the structural and sedimentological elements in the basin, and integrating our results with the previous studies, we aim to synthesise, for the first time, the onshore-offshore Oligocene – Miocene evolution of the Levant basin and its surroundings.

3. Main Structural Elements in the Deep Levant Basin

The main structural elements found in the study area are described here are: (1) the Jonah High, (2) the Leviathan, and (3) a WSW-ENE-striking strike-slip fault system. As these seems to control sedimentary patterns in the region of interest, we provide a brief description below.

The *Jonah High* is a large (~4 km high, ~13 km long, ~12 km wide) triangular structure located in the centre of the Southern Levant Basin (Figure 2). The structure extends upwards from the basement and terminates within the Late Burdigalian sedimentary sequence (Unit 7a, see below), onlapped by Oligocene – Miocene strata (Figure 2). It has been suggested that this structure represents: a large mud diapir overlying a volcanic intrusion (Ben-Gai, 2021), a rift-related basement structure (Gardosh et al., 2008b; Steinberg et al., 2018), and a Jurassic seamount that was only buried in the Early Miocene (Sagy et al., 2015).

The *Leviathan High* is a semi-triangular high controlled by buried rift-related structures (Karcz et al., 2019) (Figure 1). Joffe et al. (2022) showed the high was reactivated in the Mid Miocene (Burdigalian), with its final geometry being controlled by the LTK fault to the north (see below) and a large NE-plunging monocline (Figure 1).

Previously shown by Joffe et al. (2022), a significant WSW-ENE-striking strike-slip fault is traversing through the northern part of the Leviathan High (Figure 1). We will show here that this fault is not bounded to the Leviathan High alone, but traverse through the Tanin and Karish gas fields. For simplicity we here describe this WSW-ENE-striking strike-slip faults the LTK-fault (Leviathan – Tanin – Karish) (Figure 1). As we will show in the following sections, the LKT has at least one additional splay which traverse to the NE (LTK-North), and an additional sub-parallel WSW-ENE-striking fault which crosses through the Leviathan and Tamar (LTa fault) are also present in the study area.

4. Geological Settings

A concise review of the geological setting and history, primarily focused on the Oligocene – Miocene, is provided below (see Figure 3 for a reference tectono-stratigraphic chart). We refer the reader to excellent reviews that span periods before and after the time of interest throughout the text (e.g. Garfunkel et al., 1998, 2004; Robertson et al., 2007; Gardosh et al., 2008, 2010; Steinberg et al., 2018, and others).

4.1. Pre Oligocene – Miocene

A NE-trending rift across the Eastern Mediterranean was formed due to NW-SE extension during the Permian, Triassic, and Early Jurassic (Garfunkel and Derin, 1984; Garfunkel, 1998; Gardosh & Druckman, 2006; Robertson, 2007; Gardosh et al., 2008, 2010; Sagy et al., 2015; Granot, 2016; Sagy and Gvirtzman, 2023). Rifting was followed by a tectonic hiatus which lasted until the Late Cretaceous, and the establishment of passive margin conditions (Garfunkel and Derin, 1984; Garfunkel, 1998; Robertson, 2007; Sagy et al., 2015; Granot, 2016; Steinberg et al., 2018). A north-dipping subduction zone along the southern margin of the Cyprus Arc was created by convergence between the African and Eurasian plates in the Late Cretaceous (e.g., Santonian – Maastrichtian; Guiraud & Bosworth, 1997; Bosworth et al., 2008). Subsequence inversion-related folding continued through the Early Eocene, when large-scale transgression caused deposition of deep-water chalk and marls across much of the Middle East (Krenkel, 1924; Freund 1975; Ziegler, 2001; Garfunkel, 2004; Sagy et al., 2018; Steinberg et al., 2018).

4.2. Oligocene – Early Miocene (Aquitanian)

4.2.1. Regional Tectonics

The Oligocene marks the beginning of significant re-organisation of the basin surroundings, mostly due to the rise of the Afar Plume (31 – 29 Ma; Bosworth et al., 2005; 2015). To the east, plume related activity had caused the rise and exposure of the Eocene Arabian carbonate platform (Ziegler, 2001; Bosworth et al., 2015; Bar et al., 2016; Faccenna et al., 2019). Additionally, the rise of the Afar Plume played a significant role in the separation of the African and Arabian plates, the rise of the Ethiopian Plateau, and the initiation of NE-SW extension, eventually leading to the Red-Sea rifting (main pulse at ~25 - ~23 Ma; Stockli and Bosworth, 2019).

To the north, the NE-SW extension also triggered the Azraq-Sirhan rift (also called the Irbid rift) (~25 - ~21 Ma; Oren et al., 2023; Wald et al., 2019); a NW-trending failed rift located ~500 km north of, and sub-parallel to, the Red-Sea rift (Shaliv, 1991; Schattner et al., 2006a; Segev et al., 2014; Wald et al., 2019; Oren et al., 2023). Early Miocene faulting along the NW margin of the Azraq-Sirhan Graben was accompanied by emplacement of NW-trending dikes and related volcanism (Hatzor and Reches, 1990; Shaliv, 1991; Segev et al., 2014). The north-western-most extension of Azraq-Sirhan rift is termed the Carmel-Gilboa Fault System; a NW-striking, ~75 km-long transtensional fault zone, which forms the boundary between the northern and southern blocks of the Sinai Plate (Figure 1; Schattner et al., 2006b; Dembo et al., 2015; Gomez et al., 2020; Hamiel et al., 2022; Oren et al., 2023;). North of the Carmel-Gilboa Fault System, onshore Israel, the ~35 km-wide Galilee deformation zone (Figure 1) is dissected by similarly striking NW-SE normal faults (Gomez et al., 2020). Unlike the Red Sea rift, the Azraq-Sirhan rift did not completely spread and create oceanic crust (Wal et al., 2019).

Extension along the Red Sea formed a regional E-W, to ENE-WSW-strike-slip fault system termed the Sinai-Negev Shear Zone (Weinberger et al., 2020). The timing of the strike-slip movement ranges from Chattian – Aquitanian (27 – 22 Ma, with intense activation at 19 – 20 Ma; Bar et al., 1974; Weinberger et al., 2020), to Burdigalian (~20.5 Ma; Moustafa et al., 2014). Faulting in this zone was preceded by prominent folding that created a series of asymmetric, NE-trending anticlines, dissected by a dense network of NW-SE-striking normal faults (Moustafa et al., 2014). The geometric relationship between the NW-SE-striking normal faults and the WSW-ENE-striking dextral fault segments suggests extensional strain between the strike-slip segments (Moustafa et al., 2014).

Further north, onshore Israel, vertical motions exposed submerged rocks for denudation, eventually creating the Oligocene Truncation Surface (Avni et al., 2012). The Oligocene Truncation Surface records an uplift of >1 km of the Negev Desert, the southern Sinai Plate by >2.5 km, and the Red Sea Mountain range by >2 km. Uplift was also recorded further north, through a series of structural steps along Israel's continental margin (Bar et al., 2013, 2016). These steps indicate a vertical uplift of >500 m of the Judea Hills in three distinct phases (Late Eocene to Early Oligocene; Early to Late Oligocene; Early to Middle Miocene; Bar et al., 2016).

4.2.2. Sedimentation and Stratigraphy

Uplift and erosion across much of the southern continental Levant (southern Israel, Jordan, Sinai, and the Eastern Desert of Egypt), resulted in the regionally prominent low-relief, Oligocene Truncation Surface (*sensu* Avni et al., 2012). Scant data from limited outcrops and onshore wells suggest that the Oligocene saw some marine carbonate deposition, though the period was by far dominated by extensive erosion (Buchbinder et al., 2005; Schattner et al., 2006a; Avni et al., 2012). Offshore, in the deep Levant Basin, clastic deposition was predominantly unconfined and generally isopachous (Gardosh et al., 2008a; Joffe et al., 2022). Concurrent to the unconfined settings, the first of four significant incision events had started in the Rupelian (Early Oligocene), as indicated by buried canyon system (e.g. El Arish, Afiq, Ashdod) (Druckman et al., 1995; Buchbinder et al., 2005; Gardosh and Druckman, 2006; Gardosh et al., 2008a; Avni et al., 2012).

4.3. Middle-Late Miocene

Middle-Late Miocene was a tectonically active time in the Levant Basin related to the collision between Africa and Eurasia and subsequent southward migration of the Cypriot subduction arc southward (Gao et al., 2020 and references therein). The collision was also manifested by shallow-water, Early Miocene carbonates and onlapping of the adjacent Miocene sediments to the Eratosthenes Seamount, documenting a ~1 km uplift during the Aquitanian – Burdigalian (Robertson et al., 1998b; Gao et al., 2020).

Coevally, the Dead-Sea transform became active at its southern end, adjacent to the Gulf of Aqaba (~18 Ma; Nuriel et al., 2017), propagating northward to displace the Azraq-Sirhan Graben at ~16Ma and create a triple-junction (Oren et al., 2023), with further northward propagation documented at the southern end of the Lebanese restraining bend during ~14 Ma (Oren et al., 2020). Some suggest the locking of the strike-slip movement along the Continental Margin Fault Zone along the eastern margin of the Levant Basin resulted in the eastward jump in stress onto, and the activation of, the Dead-Sea transform (Freund, 1975; Garfunkel, 1997; Gvirtzman & Steinberg, 2012; Segev et al., 2014; Nuriel et al., 2017). The sinistral movement along the northern section of the Dead-Sea transform had isolated the Galilee from the rest of the Azraq-Sirhan Graben-related basins on the eastern side of the transform (Schattner et al., 2006a; Wald et al., 2019).

Alongside the final closure of the Indian Ocean – Mediterranean Seaway in the Aquitanian (Bialik et al., 2019; Torfstein and Steinberg, 2020), and the activation of the Miocene Syrian Arc folding event (Robertson, 1998a; Gardosh et al., 2008a; Needham et al., 2017; Sagy et al., 2018), the offshore Oligocene – Miocene strata was also dissected by thin-skinned NW-SE-striking normal faults during the Burdigalian (Ghalayini et al., 2017; Libby, 2017; Ghalayini and Eid, 2020; Joffe et al., 2022). Joffe et al. (2022) suggested a genetic connection between the normal faults and a large, WSW-ENE-striking, dextral strike-slip fault located in the centre of the Levant Basin (see map and further details in 8.1.2.2.). A similar relationship between NW-SE-striking normal faults and a WSW-ENE-striking strike-slip faults was documented south of the Levant Basin, onshore Sinai, along the Sinai-Negev Shear Zone (Moustafa et al., 2014) (see map and further details in 8.2.).

Onshore, the Tortonian marks a change in the state of stress in the Galilee. From the ~35 km wide fault zone, stress was now concentrated along the Carmel Fault (Hatzor & Reches, 1990; Schattner et al., 2006a; Wald et al., 2019). The offshore extent of the Carmel Fault is still debated, but Schattner et al., 2006b had suggested it curved N-NE along the basin margin (Figure 17). Faulting was also documented along the Or-Akiva fault, marking the end of southern end of the Carmel Fault zone (Figure 17; Steinberg et al., 2010).

Geodynamic quiescence seemed to prevail by the onset of the Messinian Salinity Crisis in the Late Miocene (Hsü et al., 1977; Ryan, 2009). Onshore, the final phase of uplift of the Judean Hills and subsidence along the Dead-Sea transform during the Pliocene disconnected the Arabian drainage system from the Levant Basin, which gave rise to an inland basin along the transform (Garfunkel, 1981; Gardosh et al., 2008a, 2008b; Gvirtzman et al., 2014).

4.3.1. Sedimentation and Stratigraphy

Miocene uplift and erosion across southern Israel, Sinai and Arabia created the vast Hazeva River, which boasted a drainage of over 100,000 km^2, spanning across western Jordan, southern Israel (Negev Desert) and eastern Sinai (Calvo & Bartov, 2001; Zilberman & Calvo, 2013; Ben-Israel et al., 2020). The Hazeva fluvial lacustrine system was deposited in part during tectonic activity (syn-kinematic), showing significant tectonic-related thickness changes across the Sinai-Negev Shear Zone (Calvo & Bartov, 2001). The sediments related to this vast river system are thicker than 2 km in places, and there is evidence of NW directed flow (Zilberman & Calvo, 2013). In northern Israel, a similar fluvial-lacustrine, NW-directed system transported eroded sediments from the exposed northern shoulders of the Red-Sea to the Levant, confined to the subsiding Izraq-Sirhan rift, with the related deposits represented by the syn-tectonic Hordos Formation (Shaliv, 1991; Morag, 2019; Wald et al., 2019; Hamiel et al., 2022).

Coeval to the deposition of the Hordos Formation, the Harrat Ash-Shaam volcanic field erupted in and around the Azraq-Sirhan rift, throughout Syria, northern Jordan, and Israel (Figure 15) (Segev et al., 2014 and references therein). Located at the NW-edge of the Harrat Ash-Shaam volcanic field, the Lower Basalt formation (17.5 – 10Ma), were extruded throughout the Galilee through NW-SE-trending dikes (Shaliv, 1991; Rozenbaum et al., 2014; Wald et al., 2019). The Lower Basalt accumulated a 650 m thick section in the Galilee, intruding into the contemporaneous upper section of the Hordos Formation. The isolation of the Galilee from the rest of the Azraq-Sirhan rift was manifested by older volcanism ages relative to the rest of the Harrat Ash-Shaam volcanic field (i.e., 17 Ma relative to 14 Ma east of the Dead-Sea transform), and longer lasting NE-SW extensional stresses (Wald et al., 2019).

In central Israel, along the Levant margin, coeval with the deposition of the Hazeva Group, rejuvenation of Early Oligocene canyon incision occurred across the Levant margin during the Burdigalian, Langhian-Serravallian, and Late Tortonian along the El Arish, Afiq and Ashdod canyons (Buchbinder et al., 1993; Druckman et al., 1995; Gardosh et al., 2008a; Gvirtzman et al., 2014). Borehole data through the Afiq Canyon suggest these were submarine rather than subaerial incision events (Druckman et al., 1995). Between these incision events, transgressions resulted in the deposition of reef buildups (Ziqlag and Pattish Formations), which were used to reconstruct sea-level changes (Buchbinder et al., 1993; Druckman et al., 1995). The initiation of the Dead-Sea transform and creation of an inland basin suggest a complete cut-off from Arabian sources into the Levant Basin occurred during the Langhian (i.e., ~16 – 14 Ma; Bar and Zilberman, 2016).

Offshore, siliciclastic Miocene strata accumulated continuously in the deep basin (Steinberg et al., 2011; Joffe et al., 2022). Rapid deposition (peaking at ~900 m/Myr in the Early Miocene) and the accumulation of thick. Sedimentary sequences were attributed to a mostly Nile-derived source (Steinberg et al., 2011; Macgregor, 2012; Gvirtzman et al., 2014; Torfstein & Steinberg, 2020). The Early Burdigalian marks the shift from sandstone-dominated to marl-dominated sequences (Figure 3) (Torfstein and Steinberg, 2020; Joffe et al., 2022;). Assuming these sands arrived from Africa (rather than Arabia), the reduction in sand content in the Late Burdigalian – Langhian was attributed to the activation of the NW-striking Temash – Baradwill trend offshore Sinai at 17 Ma, which acted as a barrier for the Nile derived sediments (Steinberg et al., 2011; Macgregor, 2012; Gvirtzman et al., 2014; Torfstein & Steinberg, 2020).

Glazer et al. (2023) shows the source of the Early Burdigalian sandstone-bearing interval is mostly Arabian, rather than African (Figure 3). A dominant Arabian source is also connected to the Azraq-Sirhan rift related subsidence and rejuvenation of incision events along the Levant continental margin (Figure 14) (Shaliv, 1991; Zilberman & Calvo, 2013). Langhian evidence comes from a mostly mudstone dominated system with scattered deep-water carbonate beds (<5 m thick) and correlates with the second uplift phase of the Judean Hills, in which the Ziqlag formation was deposited along the western flanks of the Judean Hills (Buchbinder et al., 1993; Buchbinder & Zilberman, 1997; Bar et al., 2016).

The rise and fall in sedimentation rates correlate well with the timing of exhumation pulses along the eastern flank of the Suez rift at 25 – 18 Ma, followed by a decrease in exhumation at ~18 Ma (Morag et al., 2019). The main depositional systems recorded in the deep Levant Basin were unconfined, fan-like clastic bodies (Needham et al., 2017; Stearman et al., 2021), which prevailed throughout the Oligo – Miocene, punctuated only by a brief period of Langhian carbonate deposition (Needham et al., 2017; Torfstein & Steinberg, 2020; Stearman et al., 2021).

4.3.2. *Source of Siliciclastic Sediments*

A major debate regarding the source of the Oligocene – Miocene siliciclastic sediments preserved in the deep Levant Basin is still ongoing, with three competing models. The first suggests the sediments were sourced from the northern flanks of the Red Sea, traversing NW through Arabia, before being deposited within the Levant Basin through E-W-trending canyons (Buchbinder et al., 1993; Druckman et al., 1995; Gardosh et al., 2008a). The second model implied the sedimentary fill of the Levant Basin was mainly sourced by a N-trending, proto-Nile system, directing sediments through the southern flanks of the Red Sea, with the Arabian source only playing a minor role (Macgregor, 2012; Steinberg et al., 2012; Gvirtzman et al., 2014). Recently Glazer et al. (2023) suggested a new hybrid model. In this hybrid model, the Arabian source was most dominant during the Early Oligocene (Rupelian) and Early Miocene (Aquitanian – Burdigalian), whereas the Late Oligocene (Chattian), lowest Early Miocene (early Aquitanian), and Middle-Late Miocene (Tortonian, Langhian, Serravallian) were dominated by Nile-derived sediments.

Our understanding of the Levant Basin's tectono-stratigraphy has improved significantly by using 2D seismic reflection data (e.g., Gardosh et al., 2008a), forward modelling (e.g., Gvirtzman et al., 2014), and borehole cutting data (e.g., Glazer et al., 2023). We here fill the missing gap of a comprehensive study of the Oligocene – Miocene sedimentary systems using age-constrained, 3D seismic reflection and borehole data which connects onshore and offshore events.

5. Data and Methods

Our dataset consists of two 2D seismic reflection surveys and five 3D seismic reflection surveys, all of which are pre-stack depth migrated (PSDM). The five 3D surveys cover 7,841 km^2 and are generally located in deep water (~1.5 km) offshore Israel (Figure 1). The datasets were collected and reprocessed at different times, and the 3D surveys have different bin sizes (see Table 1). Large data gaps in the Leviathan and NBL data sets occur around producing gas fields. Despite these gaps, the connectivity between the surveys is very good, allowing a continuous interpretation of horizons across surveys. All surveys are zero phase, 'normal' SEG polarity, where a positive amplitude peak indicate an increase in acoustic impedance with depth (red in figures), and a negative amplitude trough a decrease in acoustic impedance (blue in figures). Despite being located below ~2.5 km of halite-rich evaporites, imaging of the Oligocene-Miocene is good, allowing for horizon and fault mapping across all the surveys.

here is a general trend of better-quality imaging northwards. Miocene horizons either onlap older strata or are cut by erosional canyons, limiting their extension to the east and south-east.

The Oligocene-Miocene seismic-stratigraphy presented here follows the Joffe et al. (2022) framework, who defined nine sub-evaporite reflections (excluding base-evaporite). Between these main intervals, iso-proportional slices were created to create sub-intervals for better refinement of the seismic events through time. These sub-horizons were used to broadly extract stratigraphically concordant slices from a RGB spectral decomposition volume. By decomposing the seismic reflection data into three frequency bands, and then blending the red-green-blue channels into a single colour map; the new RGB spectral decomposition volume highlights subtle resolution thicknesses, which allows us to determine the type, distribution, and evolution of the sedimentary features within the main stratigraphic intervals. The frequencies used (8.33, 11.82, 15.33 1/km) were chosen after testing a series of frequencies combinations and chosen as they revealed the most details across the depth of interest and different seismic surveys.

Map view observations were constrained using vertical sections through the original reflectivity volume, before facies were assessed, and paleo-geographic maps were produced. Assuming the overall channel direction was from the basin margin to its centre (i.e., from E and S), the orientation of the channels is also shown by rose diagrams. Sedimentary thickness (isopach) maps between the main seismic intervals were used as proxies for the timing of syn-depositional structural activity; specifically, across-fault thickness changes indicate faults displacing the seabed.

6. Results – Tectono-Stratigraphic Observations

In the following section we describe thickness variations within each seismic – stratigraphic intervals and the features seen in a representative extract from the spectral decomposition volumes. Intervals nomenclature follow Joffe et al. (2022) and depositional elements follow Janocko et al., (2013).

6.1. Oligocene – Early Miocene (Aquitanian)

The Oligocene – Aquitanian is the oldest interval described here. Sediment thickness is greatest in the south, but largely isopachous in the W and NW, with an average thickness of ~1500 m (Figure 4A). Thinning is observed to the east above an NNE-trending anticline (Figure 4A).

Thickness maps separating Early Oligocene (Unit 3) from Late Oligocene – Early Miocene strata (Unit 4&5) show thinning above the easterly NNE-trending anticline was only prominent during the Early Oligocene (i.e., Rupelian, Unit 3) (Figure 4B). The dominant features observed in the spectral decomposition images are ~250 m wide, and ~100 m deep, sinuous, NW-trending erosional and turbidity-like, meandering channel belts (Figure 5B and SP2-22). At the upper levels of Early Miocene (i.e., Upper Aquitanian), wider (~2.5 km wide), less sinuous channels are observed east of Jonah High (Figure 5A).

6.2. Early Burdigalian

After a period of relative isopachous deposition, the Early Burdigalian deposits shows thickness changes within our study area (Figure 6A). Whereas isopachous deposition is observed in the northern part of the study area, thinning trends are prominent towards the LTK-fault in the northwest, and east of the Jonah High (Figure 6A). The interval attains its greatest thickness, ~450 m, adjacent to Jonah High. In the south, thinning is observed to the southeast. However, this thinning is caused by post-depositional incision (see Figure 7), rather than structural uplift or variable subsidence. This post-depositional incision (~10 km wide, ~900 m deep) is bounded between the Top Aquitanian horizon (base of the Early Burdigalian seismic interval) and the Intra-Tortonian horizon (top of the Early Tortonian, see below). In cross-section the incision is highlighted by a U-shaped base. On the spectral decomposition maps, the incision is observed by bright amplitudes showing the later filling of the meandering channel-bend mounds.

6.3. Late Burdigalian

Late Burdigalian strata shows significant and regionally pervasive thickness changes associated with the NW-SE-striking normal faults (Figure 8A). On the Leviathan high, across the LTK fault, thinning is observed on the southern edge of the fault, whereas thickening is observed on the northern side (Figure 8A). A smaller north-east splay of the LTK is also associated with thickness change (Figure 9). The sub-parallel, LTKa fault crosscuts through the Leviathan and Tamar gas fields (Figure 9). In the southern end of the study area, a deep-rooted flower structure (Figure 9) and en-echelon thickness-changes are observed, trending NNE (Figure 8A).

6.4. Langhian

Besides a few NW-SE-striking instances at the northern edge of the NBL survey, the prominent across-fault thickness changes that were prevalent during the Late Burdigalian, are mostly not present during the Langhian (Figure 10A). Thinning above the Leviathan High changed in nature, from the high's flanks to dome-like above the centre of the structure (Figure 10A). Thickening is observed in the southern section of the study-area, defining the same en-echelon-like geometry seen in the Late Burdigalian maps (Figure 10).

Spectral decomposition extraction of Langhian age strata shows a bright, wide (~7 km), NW-trending feature on the eastern side of the study area (Figure 10B). Flattening the Top Langhian horizon reveals an erosional surface associated with ~200 m deep incision, which is filled with onlapped younger strata (Figure 10B).

6.5. Early Tortonian

Unlike the older intervals, the Early Tortonian sediments show a major thickening towards the west-southwest, alongside continued thinning above the Leviathan High. Early Tortonian strata cover the Jonah High, but thinning above the structure still reflects its distinct triangular shape (Figure 11A). No thickness changes are seen across the NW-SE-striking faults. As described by Joffe et al., (2022), the Early Tortonian has a distinct, discontinuous and chaotic seismic character (Figure 11B). This chaotic sequence thins towards the NNW, where it completely disappears, transitioning into a set of continuous, layered reflections (Figure 11B). Spectral decomposition slices show almost no transport elements within the chaotic sequence, but some NW-trending channels are well-imaged in its upper, well-layered area, especially within along the E-NE parts of the study area (Figure 11B).

6.6. Late Tortonian

Similarly to the Early Tortonian deposits, the Late Tortonian sediments thin above the Leviathan High. Mild thinning is also observed above the LTK area (Figure 12A). Newly published structural map of the base-Messinian Evaporites shows that the LTK fault and associated NW-SE-striking normal faults are displacing the base of salt, filling gaps in data restricted to this study (Moneron et al. 2024).

The Late Tortonian spectral decomposition slices and associated cross-sections indicate several NW-trending valleys-filled complexes incised within the older strata during that time (Figure 12). Due to their incision, these valleys are also clearly seen in the thickness map (Figure 12A).

Even if less pronounced in map-view, a significant erosional base, and younger onlapped channel fill are clearly seen on cross-section extraction (Figure 12B).

7. Discussion – Tectonic Evolution and Sediment Routing

In the following section we will use our observations of stratigraphy, channel geometries and sediment thickness to resolve the evolution of the Levant Basin in context with onshore and offshore, regional and local events.

7.1. Early Oligocene

Thickness maps presented in 7.1. show thinning above an NNE-trending anticline at the eastern part of the study area, but isopachous deposition since (Unit 3; Figure 4B). The timing of easterly thinning suggests the easterly NNE-trending anticline is related to the early Oligocene activation of the Continental Margin Fault Zone (e.g., Gvirtzman and Steinberg, 2012). Unlike Gvirtzman and Steinberg (2012), who argued the fault zone was locked in the Burdigalian, isopachous deposition since the Late Oligocene suggest that the western part of the Continental Margin Fault Zone was locked in the Late Oligocene.

The thickening depocenter, located at the southern end of the study area, aligns with the presumed Oligocene-age outlet of the Afiq canyon described by Gardosh et al. (2008a) (Figure 4B & 13). This geographical correlation is supported by both onshore provenance analysis which favoured that a Rupelian river system was sourced from the Red-Sea mountains, traversing west through Arabia and into the Levant (e.g., Glazer et al., 2023; Morag et al., 2021), and by the Hannah-1 well, which encountered Rupelian age sandstone in a large, incised canyon (e.g., Gardoshet al., 2008a) (Figure 13). Despite the lack of data from offshore Sinai to constrain any southerly source (e.g. Nile River or Sinai incision through the El-Arish canyon) transporting sediments along the continental margin; it is possible that this southerly depocenter had occurred due to the first (of three) documented Afiq Canyon incision events previously suggested from onshore studies but had not yet been identified offshore (e.g., Buchbinder et al., 2005; Gardosh & Druckman, 2006; Avni et al., 2012).

Detectable NE-trending meandering channel system, alongside the establishment of the Nile-River at 30 Ma led us to suggest that the main source of sediments in the early Oligocene (Rupelian) was mostly an easterly source, with the paleo-Nile –river system having only minor contribution in this area at that time.

7.2. Late Oligocene – Early Miocene

Predominantly isopachous deposition (Unit 4; Figure 4B) conforms with a regional tectonic hiatus during the Late Oligocene. A vast NE-trending, turbidity-like, sedimentary system that runs clear across the basin (Figure 5 and SP 9 - 22), suggests that either no tectonically driven processes were active within the basin, or sedimentation rates were much higher than any tectonic processes. This observation supports Torfstein and Steinberg (2020) sedimentation rates from well-data, who showed the Late Oligocene – Early Miocene had the highest rates of deposition. These observations also conform with Glazer et al. (2023) who suggested an African dominated source for the Late Oligocene deposition in the Levant Basin (Figure 3).

Notably, onshore observations suggest that Lower Hazeva members of similar age, consisting of gravel and sandstone sediments, were transported towards the Levant during an Oligocene tectonic hiatus (e.g., Calvo & Bartov, 2001; Zilberman & Calvo, 2013). Unlike Glazer et al. (2023) we do not see any difference between the Upper Oligocene and Aquitanian (Lower Miocene) intervals, in terms of structural or sedimentological features. We do not see any evidence for a northerly source, in agreement with Glazer et al. (2023).

7.3. Early Burdigalian

Structurally, thinning trends towards both LTK fault and the easterly anticline, but relative isopachous deposition throughout the study area indicate initial folding and activation of these two structures (Figure 6). These thinning trends resemble the folding documented onshore Sinai at the early stages of activation of the similarly-trending Sinai-Negev Shear Zone (post 20.5 Ma) (Moustafa et al., 2014; Moustafa, 2020) (Figure 14).

The location of the large Late Miocene incision highlighted in Figure 7, suggests it is the deep offshore extension of the Afiq Canyon (Figure 14). Additionally, westward paleo-flow analysis on the similar-aged Rotem Member (Zilberman and Calvo, 2013), alongside its mineralogical similarity to the equivalent stratigraphic interval offshore (Glazer et al., 2023), suggests that the Early Burdigalian deposits are, at least in part, an offshore extension to the onshore Rotem Member. In northern Israel, the Hordos formation was also flowing towards the Levant Basin along the Azraq-Sirhan paleo-valley through ta northerly pathway, which is not imaged in this study (Figure 14). The occurrence of several N-S trending channels (Figure 6B & 14), NE-trending channels (Figure 6B & SP23 - 27), alongside small, NE-trending fan-like features (at least two we highlighted in Figure 6), and the extension of the Afiq canyon suggest that the

Early Burdigalian is not purely Arabian, but reflects a transition period between reducing contribution from the Nile River to increase contribution from Arabia.

Early Burdigalian also marks a tectonic transition period with several tectonic events occurring simultaneously; (1) uplift of the Eratosthenes Seamount, (2) continuation of the spreading of the Red-Sea (i.e., main phase of exhumation, 25-18 Ma), (3) the propagation of the Azraq-Sirhan rift, (4) the inception of the Dead-Sea transform fault system, (5) de-activation of the Continental Margin Fault Zone, and (6) the activation of the Negev-Sinai Shear Zone (19-20 Ma) (Figure 14). We therefore suggest that across the Levant Basin and its surrounding, the Early Burdigalian time was a transition period both from a tectonic and sedimentary perspective.

7.4. Late Burdigalian

Structurally, thickness changes across the basin show the NW-SE-striking, layer-bound normal fault system occurs across the Southern Levant Basin, based on a compilation of our observations with previous mapping from the Norhtern Levant Basin (e.g., Ghalayini et al., 2017; Libby, 2017; Ghalayini and Eid, 2020) (Figure 15). Thickness changes are found across the study area, including across the LTK, LTK-north, LTa, and the southern en-echelon system. Taken together, these thickness changes map the architecture of the strike-slip fault system in the Levant Basin (Figure 9). The scope and variability of these features suggest that the mechanism of the NW-SE-striking normal faults system might be more complex than previously thought (Figure 15). Our offshore observations correlate with contemporaneous strike-slip movement, folding, and perpendicular faulting onshore the Sinai Peninsula. We therefore suggest a movement along the similarly striking offshore WSW-ENE-striking LTK fault, and that these contemporaneous movements may have all been genetically related.

Reduction in the amount of sandstone in the Burdigalian is documented in offshore wells (e.g., Torfstein & Steinberg, 2020), and was thought to indicate a decrease in the amount of sand transported to the basin through Nile River due to the activation of the Temash-Bardawill Trend (Figure 15). We did not observe any N-S-trending channel systems, suggesting that the southerly source was not active during that time, or it is not well imaged (Figure 15 and SP 28-32). Wave-like features on the eastern side of the SMA survey show onlaps and stacking patterns, which could be either sediment-waves or some sort of small-scale delivery system that might have contributed sand to the basin (Figure 8B). Continued deposition of sandstoneprone Rotem Member onshore, renewed onshore and margin incision, and NW-trending offshore channels indicate that sand either continued to arrive to the basin, even if the amount decreased significantly, or bypassed the well-data provided by Joffe et al. (2022) and Glazer et al. (2023) (Figure 15).

7.5. Langhian

Unlike the Late Burdigalian deposits, thickness changes across the NW-SE-striking normal faults only appear in the Langhian at the northern-most parts of the NBL survey. The activation of only the northern faults, but lack of any thickness changes across the other datasets could potentially suggest a northward propagation of stress through time, i.e., diachronous propagation of the NW-SE-striking faults between the southern and northern Levant Basin. We relate the northward strain propagation to the similar strain distribution along the Dead-Sea transform (e.g., Nuriel et al., 2017; Oren et al., 2020). The sinistral movement along the transform had mostly migrated from its southern section (along the Suez-Rift) to its northern section (branching of the transform into the Levant Fracture System) during this time (Oren et al. 2023 and references therein), suggesting a kinematic connection between younger faults offshore and younger sinistral movement along the Dead-Sea transform.

Other thickness changes in this interval are associated with dome-like thinning geometries above the Leviathan High and a small anticline at SMA (Figure 10A). These thinning geometries could be associated with either differential compaction or regional folding. Trying to discriminate between the two is beyond the scope of this manuscript, but we highlight these thinning events concur during the active folding event of the Syrian Arc II (Miocene shortening event) (Figure 16).

Despite well data suggesting that the Langhian is mostly sandstone-poor (e.g., Torfstein & Steinberg, 2020; Joffe et al., 2022), Figure 10B shows a large, incised canyon seen as bright reflections both in map and cross-section view. Based on its location and extent we interpret the large NW-trending incision event to be the offshore extension of the Ashdod canyon (Gardosh et al. 2008a) (Figure 16). As both the Ashdod (e.g. Figure 10) and Afiq (e.g. Figure 7) canyons are active at this time, and no N-S/NE-SW-trending channels are observed, we assume that the main source of sand to the basin were an easterly source through the incised canyons (Figure 16).

Notably, our results here differ from Glazer et al. (2023) who suggested that the few sandstone show in the basin were mainly sourced from Africa during that time. These differences could potentially be a result of the sample locations of the sparse wells, which targeted structural highs, or potentially missed the seismically imaged large channels. The lack of Serravallian sediments in most of the wells in the basin was associated with a regional hiatus throughout the basin and has been suggested to correlate with the Miocene Carbonate Crash (MCC) (Torfstein and Steinberg, 2020).

7.6. Early Tortonian

The chaotic seismic characteristic of the Early Tortonian deposits stands out in the sedimentary sequence in the Levant Basin, with the origin of this chaotic interval is currently unknown. Thrusting within the interval suggest it is likely to be a very large-scale mass transport complex, but as we do not see or know of any Tortonian age headwall scarp, or where these sediments originated, it is hard to say for sure. Documentation of similar age chaotic section were described along the Rosetta Fault, offshore the western Nile delta, Herodotus Basin (El-Fattah et al., 2021), the eastern slopes of the Eratosthenes Seamount and onshore Cyprus (Papadimitriou et al., 2018 and references therein). The latter suggested that the source of these onshore deposits would be a catastrophic event occurred due to a large-scale seismic event created by the collision between the Eratosthenes Seamount and the island of Cyprus. A general south-west thickening trend, alongside the NNE-trending channels indicate the Early Tortonian was dominated by an African source, in agreement with Glazer et al. (2023) (Figure 17). The exact source of the chaotic unit is beyond the scope of this manuscript. We suggest that it was either sourced from the Eratosthenes-related catastrophic event, or by a rapid propagation of the Nile Delta at that time.

7.7. Late Tortonian

Continued thinning above the Leviathan High during the Late Tortonian (Unit 10) could still be associated with Syrian Arc related folding, but the thinning above the Jonah High is puzzling (Figure 12A). The Syrian Arc structures are normally described as asymmetrical anticlines, but the unique triangular shape of the Jonah High shows no sign of inversion or folding (Figure 12A). The interpretation of these thinning geometries depends on the interpretation of the origin of the Jonah High structure. On the one hand, if this is a large mud-diapir (e.g. Ben-Gai, 2021), then thinning above it would suggest a time of upward motion and diapirism. However, as no folding is seen on the older strata adjacent to the structure (i.e., no minibasins style deformation), it would be hard to explain it as such a diapir. On the other hand, if the structure is an old structure located high above the basin (i.e., remnant of a rift fragment or a Jurassic seamount, a volcanic structure, or a carbonate buildup; Gardosh et al., 2008b; Sagy et al., 2015; Steinberg et al., 2018) it is possible that the thinning present in the Langhian and Tortonian are created by differential compaction.

Consistent with our results (Figure 12A), the newly published structure map of the base of Messinian Evaporite (Moneron et al., 2024; their figure 3A) sheds light of the activation of the LTK strike slip fault and the associated NW-SE-striking normal faults. It shows that the NW-SE-normal faults are only seen along the LTK fault in an en-echelon geometry, strengthening the genetic connection described by Joffe et al. (2022) between the LTK fault and the NW-SE-striking normal faults. The activation of this large strike-slip fault and its connection to the NW-SE-striking normal faults may be the missing link between the faults in the Southern Levant Basin and the Northern Levant Basin. Whereas the former does not continue above the Early Tortonian, the latter displace the base-of salt reflector.

8. Summary

This study shows that sedimentation in the deep Levant Basin during the Early Oligocene was dominated by an easterly (Arabian) source through incised canyon valleys (Figure 13), but that subsequently during the Late Oligocene to Aquitanian, it became dominated by a southerly (African) source. This is supported by a dense system of turbidity currents and isopachous deposition at that time (Figure 5). This change in sediment source could have been caused by the breakup of Africa and Arabia, which raised the Ethiopian Plateau and caused the nucleation of the Nile River.

The Burdigalian marks a major change in the structural and sedimentological elements in the basin and surrounding area (Figure 14). Structurally, early folding adjacent to the LTK fault, like concurrent onshore Sinai folding matches an initial northward propagation of the Dead-Sea transform at that time (Figure 14). Stratigraphically, renewed canyon incision from the margins to the east (Figure 7 & 14), deposition of the NW-flowing Hordos formation, and turbidite channels flowing northward in the basin, indicate that the Early Burdigalian was probably dominated by an Arabian source, but also had significant contribution from Africa. The Late Burdigalian was controlled by a large-scale NW-striking normal faulting across the basin, with similar faulting also occurred onshore the Sinai anticlines. Renewed incision of the

Arabian-sourced incision of the Afiq canyon alongside northward propagation of the Dead-Sea transform (Figure 15).

The Langhian deposits show folding above the Leviathan High, with normal faulting mostly ended across the southern Levant Basin, with exception of the northern-most part of the study area. Published borehole data showed that Langhian deposits is stratigraphically mudstone dominated, but with wide-spread carbonate deposition offshore and on the basin-margin (Ziqlag formation) (Figure 16). The Early Tortonian marks a possible large-scale catastrophic event throughout the Eastern Mediterranean, along with a return to a southerly source (Figure 17). Lastly, the Late Tortonian is controlled by large-scale incised valleys and a return to an easterly source.

9. Conclusion

By integrating multiple high-quality 3D seismic reflection surveys, thickness maps, ISO-proportional slices, and spectral-decomposition, we characterise the structural and sedimentological elements in the Levant Basin, offshore Israel. We have integrated our offshore results to known onshore/regional events to create a coherent evolutionary model for the region. Our results allowed us to demonstrate the geographical dispersion of the different sedimentary intervals in 3D, therefore establishing a model for the role evolving tectonics of the regional plates play in the alternation of sediment sourcing into the Levant Basin.

References

Avni, Y., Segev, A., & Ginat, H. (2012). Oligocene regional denudation of the northern Afar dome: Pre- and syn-breakup stages of the Afro-Arabian plate. GSA Bulletin, 124(11–12), 1871–1897. https://doi.org/10.1130/B30634.1

Bar, M., Kolodny, Y., Bentor, Y.K., 1974. Dating faults by fission track dating of epidotesan attempt. Earth Planet. Sci. Lett. 22 (2), 157–162.

Bar, O., Gvirtzman, Z., Feinstein, S., & Zilberman, E. (2013). Accelerated subsidence and sedimentation in the Levant Basin during the Late Tertiary and concurrent uplift of the Arabian platform: Tectonic versus counteracting sedimentary loading effects. Tectonics, 32(3), 334–350. https://doi.org/10.1002/tect.20026

Bar, O., Zilberman, E., Feinstein, S., Calvo, R., & Gvirtzman, Z. (2016). The uplift history of the Arabian Plateau as inferred from geomorphologic analysis of its northwestern edge. Tectonophysics, 671, 9–23. https://doi.org/10.1016/j.tecto.2016.01.004

Bar, O., & Zilberman, E. (2016). Subsidence and conversion of the Dead Sea basin to an inland erosion base level in the early middle Miocene as inferred from geomorphological analysis of its ancient western fluvial outlet. Geomorphology, 261, 147–161. https://doi.org/https://doi.org/10.1016/j.geomorph.2016.02.028

Ben-Gai, Y. (2021). The world unique triangular shaped Jonah High in the Levant Basin, eastern mediterranean – Tectonic setting, stratigraphy and exploration considerations. Marine and Petroleum Geology, 105206. https://doi.org/https://doi.org/10.1016/j.marpetgeo.2021.105206

Ben-Israel, M., Matmon, A., Hidy, A. J., Avni, Y., and Balco, G.: Early-to-mid Miocene erosion rates inferred from pre-Dead Sea rift Hazeva River fluvial chert pebbles using cosmogenic 21Ne, Earth Surf. Dynam., 8, 289–301, 2020. https://doi.org/10.5194/esurf-8-289-2020

Bialik, O. M., Frank, M., Betzler, C., Zammit, R., & Waldmann, N. D. (2019). Two-step closure of the Miocene Indian Ocean Gateway to the Mediterranean. Scientific Reports, 9(1), 1–10. https://doi.org/10.1038/s41598-019-45308-7

Bosworth, W., Huchon, P., & McClay, K. (2005). The Red Sea and Gulf of Aden Basins. Journal of African Earth Sciences, 43(1), 334–378. https://doi.org/https://doi.org/10.1016/j.jafrearsci.2005.07.020

Bosworth, W., El-Hawat, A. S., Helgeson, D. E., & Burke, K. (2008). Cyrenaican "shock absorber" and associated inversion strain shadow in the collision zone of northeast Africa. Geology, 36(9), 695-698. https://doi.org/10.1016/S0040-1951(97)00212-6

Bosworth, W., Stockli, D. F., & Helgeson, D. E. (2015). Integrated outcrop, 3D seismic, and geochronologic interpretation of Red Sea dike-related deformation in the Western Desert, Egypt – The role of the 23Ma Cairo "mini-plume." Journal of African Earth Sciences, 109, 107–119. https://doi.org/https://doi.org/10.1016/j.jafrearsci.2015.05.005

Bouma, A.H. (2005). Key controlas on the characteristics of turbidite systems. In: Lomas, S.A., Joseph, P. (Eds.), Confined Turvidete Systems. Geological Society Spcial Publication 222. The Geological Society, London, 9-22. https://doi-org.iclibezp1.cc.ic.ac.uk/10.1144/GSL.SP.2004.222.01.02

Buchbinder, B., Calvo, R., & Siman-Tov, R. (2005). The Oligocene in Israel: A marine realm with intermittent denudation accompanied by mass-flow deposition. Israel Journal of Earth Sciences, 54(2).

Buchbinder, B., Martinotti, G. M., Siman-Tov, R., & Zilberman, E. (1993). Temporal and spatial relationships in Miocene reef carbonates in Israel. Palaeogeography, Palaeoclimatology, Palaeoecology, 101(1), 97–116. https://doi.org/https://doi.org/10.1016/0031-0182(93)90154-B

Buchbinder, B., & Zilberman, E. (1997). Sequence stratigraphy of Miocene-Pliocene carbonate-siliciclastic shelf deposits in the eastern Mediterranean margin (Israel): effects of eustasy and tectonics. Sedimentary Geology, 112(1), 7–32. https://doi.org/https://doi.org/10.1016/S0037-0738(97)00034-1

Calvo, R., & Bartov, Y. (2001). Hazeva Group, southern Israel: New observations, and their implications for its stratigraphy, paleogeography, and tectono-sedimentary regime. Israel Journal of Earth Sciences, 50(2–4), 71–99. http://ezproxy.haifa.ac.il/login?url=https://search.ebscohost.com/login.aspx?direct=true&db=a9h&AN=14592265&site=ehost-live&scope=site

Christensen, C. J., & Powers, G. (2013). Formation Evaluation Challenges In Tamar Field, Offshore Israel. SPWLA 54th Annual Logging Symposium, 1–12.

Dembo, N., Hamiel, Y., and Granot, R. (2015). Intraplate rotational deformation induced by faults. Journal Geophysical Research Solid Earh, 120, 7308-7321. http://doi.org/10.1002/2015JB012264.

Druckman, Y., Buchbinder, B., Martinotti, G. M., Tov, R. S., & Aharon, P. (1995). The buried Afiq Canyon (eastern Mediterranean, Israel): a case study of a Tertiary submarine canyon exposed in Late Messinian times. Marine Geology, 123(3), 167–185. https://doi.org/https://doi.org/10.1016/0025-3227(94)00127-7

El-Fattah, A., Moustafa, A. R., & Yousef, M. (2021). A new insight into the structural evolution of Rosetta Fault, eastern margin of Herodotus Basin, East Mediterranean. Marine and Petroleum Geology, 131, 105161. https://doi.org/10.1016/j.marpetgeo.2021.105161

Faccenna, C., Glišović, P., Forte, A., Becker, T. W., Garzanti, E., Sembroni, A., & Gvirtzman, Z. (2019). Role of dynamic topography in sustaining the Nile River over 30 million years. Nature Geoscience, 12(12), 1012–1017. https://doi.org/10.1038/s41561-019-0472-x

Fielding, L., Najman, Y., Millar, I., Butterworth, P., Garznati, E., Vezzoli, G., Barford, D., and Kennel, B., (2018). The initiation and evolution of the River Nile. *Earth and Planetary Science Letters*, v. 489, p. 166 - 178. https://doi.org/10.1016/j.epsl.2018.02.031

Freund, R. (1975). The Triassic-Jurassic structure of Israel and its relation to the origin of the eastern Mediterranean. Geological Survey of Israel.

Gao, H., Wen, Z., Shi, B., Wang, Z., & Song, C., (2020). Tectonic characteristics of the Eratosthenes Seamount and its periphery: implications for the evolution of the eastern Mediterranean. Marine Geology, 428, 106266. https://doi.org/10.1016/j.margeo.2020.106266

Gardosh, M. A., & Druckman, Y. (2006). Seismic stratigraphy, structure and tectonic evolution of the Levantine Basin, offshore Israel. Geological Society, London, Special Publications, 260(1), 201. https://doi.org/10.1144/GSL.SP.2006.260.01.09

Gardosh, M., Druckman, Y., Buchbinder, B., & Calvo, R. (2008a). The Oligo-Miocene deepwater system of the Levant Basin. In Geological Survey of Israel (Issue December). Geological Survey of Israel. https://doi.org/GSI/33/2008

Gardosh, M., Druckman, Y., Buchbinder, B., & Rybakov, M. (2008b). The Levant Basin Offshore Israel: Stratigraphy, Structure, Tectonic Evolution and Implications for Hydrocarbon Exploration - revised edition. Geological Survey of Israel report GSI/4/2008 (Issue April). Geological Survey of Israel.

Gardosh, M. A., Garfunkel, Z., Druckman, Y., & Buchbinder, B. (2010). Tethyan rifting in the Levant Region and its role in Early Mesozoic crustal evolution. Geological Society, London, Special Publications, 341(1), 9-36. https://doi.org/10.1144/SP341.2

Garfunkel, Z. (1981). Internal structure of the Dead Sea leaky transform (rift) in relation to plate kinematics. Tectonophysics, 80(1–4), 81–108. https://doi.org/10.1016/0040-1951(81)90143-8

Garfunkel, Z. (1997). The history and formation of the Dead Sea basin. In T. M. Niemi, Z. Ben-Avraham, & J. R. Gat (Eds.), The Dead Sea, the Lake and its Setting (Issue 36, pp. 36–56). Oxford University Press, USA.

Garfunkel, Z. (1998). Constrains on the origin and history of the Eastern Mediterranean basin. Tectonophysics, 298(1–3), 5–35. https://doi.org/10.1016/S0040-1951(98)00176-0

Garfunkel, Z. (2004). Origin of the Eastern Mediterranean basin: A reevaluation. Tectonophysics, 391(1-4 SPEC.ISS.), 11–34. https://doi.org/10.1016/j.tecto.2004.07.006

Garfunkel, Z., & Derin, B. (1984). Permian-early Mesozoic tectonism and continental margin formation in Israel and its implications for the history of the Eastern Mediterranean. Geological Society Special Publication, 17(1), 187–201. https://doi.org/10.1144/GSL.SP.1984.017.01.12

Ghalayini, R., & Eid, C. (2020). Using polygonal layer-bound faults as tools to delimit clastic reservoirs in the Levant Basin offshore Lebanon. AAPG Bulletin, 104(3), 629–656. https://doi.org/10.1306/07151918155

Ghalayini, R., Homberg, C., Daniel, J. M., & Nader, F. H. (2017). Growth of layer-bound normal faults under a regional anisotropic stress field. Geological Society, London, Special Publications, 439(1), 57 LP – 78. https://doi.org/10.1144/SP439.13

Glazer, A., Avigad, D., Morag, N., & Gerdes, A. (2023). Tracing Oligocene− Miocene source-to-sink systems in the deep Levant Basin: A sandstone provenance study. GSA Bulletin. https://doi.org/10.1130/B36864.1

Gomez, F., Cochran, W.J., Jaafar, R., Reilinger, R., Floyd, M., King, R.W., and Barazangi, M. (2020). Fragmentation of the Sinai Plate indicated by spatial variation in present-day slip rate along the Dead Sea Fault System. Geophysical Journal International, 221, 1913-1940. https://doi.org/10.1093/gji/ggaa095.

Guiraud, R., & Bosworth, W. (1997). Senonian basin inversion and rejuvenation of rifting in Africa and Arabia: synthesis and implications to plate-scale tectonics. Tectonophysics, 282(1-4), 39-82. https://doi.org/10.1016/S0040-1951(97)00212-6

Granot, R. (2016). Palaeozoic oceanic crust preserved beneath the eastern Mediterranean. Nature Geoscience, 9(9), 701–705. https://doi.org/10.1038/ngeo2784

Gvirtzman, Z., & Steinberg, J. (2012). Inland jump of the Arabian northwest plate boundary from the Levant continental margin to the Dead Sea Transform. Tectonics, 31(4), n/a-n/a. https://doi.org/10.1029/2011TC002994

Gvirtzman, Z., Csato, I., & Granjeon, D. (2014). Constraining sediment transport to deep marine basins through submarine channels: The Levant margin in the Late Cenozoic. Marine Geology, 347, 12–26. https://doi.org/10.1016/j.margeo.2013.10.010

Hamiel, Y., Katz, O., Avni, A. (2022). Migration and localization of faulting near the intersection of the Dead Sea Fault and the Carmel-Gilboa-Faria Fault System. GSA Bulletin, 135(5-6), 1310-1326.

Hatzor, Y., and Reches, Z. (1990). Structure and paleostresses in the Gilboa' region, western margins of the central Dead Sea rift. Tectonophysics, 180, 87-100. http://doi.org/10.1016/0040-1951(90)90374-H.

Howlett, D. M., Gawthorpe, R. L., Ge, Z., Rotevatn, A., & Jackson, C. A. L. (2021). Turbidites, topography and tectonics: Evolution of submarine channel-lobe systems in the salt-influenced Kwanza Basin, offshore Angola. *Basin Research*, *33*(2), 1076-1110. https://doi.org/10.1111/bre.12506

Hsü, K. J., Montadert, L., Bernoulli, D., Cita, M. B., Erickson, A., Garrison, R. E., Kidd, R. B., Mèlierés, F., Müller, C., & Wright, R. (1977). History of the mediterranean salinity crisis. Nature, 267(5610), 399–403. https://doi.org/10.1038/267399a0

Jackson, C. A. L., Barber, G. P., & Martinsen, O. J. (2008). Submarine slope morphology as a control on the development of sand-rich turbidite depositional systems: 3D seismic analysis of the Kyrre Fm (Upper Cretaceous), Måløy Slope, offshore Norway. Marine and Petroleum Geology, 25(8), 663-680. https://doi.org/10.1016/j.marpetgeo.2007.12.007

Janocko, M. N. W. H. S. W. M., Nemec, W., Henriksen, S., & Warchoł, M. (2013). The diversity of deep-water sinuous channel belts and slope valley-fill complexes. Marine and Petroleum Geology, 41, 7-34. https://doi.org/10.1016/j.marpetgeo.2012.06.012

Joffe, A., Jackson, C.-L., Steinberg, J., Bell, R. E., & Makovsky, Y. (2022). Origin and kinematics of a basin-scale, non-polygonal, layer-bound normal fault system in the Levant Basin, eastern Mediterranean. Basin Research, 00, 1– 30. https://doi.org/10.1111/bre.12729

Kanari, M., Tibor, G., Hall, J. K., Ketter, T., Lang, G., & Schattner, U. (2020). Sediment transport mechanisms revealed by quantitative analyses of seafloor morphology: New evidence from multibeam bathymetry of the Israel exclusive economic zone. Marine and Petroleum Geology, 114, 104224. https://doi.org/10.1016/j.marpetgeo.2020.104224

Karcz, K., Gellman, Y., Shitrit, O., & Steinberg, J. (2019). The Leviathan Field - Nine Years Since Discovery and Nearing First Gas. Second EAGE Eastern Mediterranean Workshop, 2019(1), 1–5. https://doi.org/10.3997/2214-4609.201903152

Krenkel, E. (1924). Der Syrische Bogen. Zentralblatt Mineralogie, 9(10), 274–281.

Libby, S. A. (2017). Implications of seismic data for the structural evolution and numerical modelling of the Eastern Mediterranean Basin [Harriot-Watt University]. http://hdl.handle.net/10399/3440

Macgregor, D. S. (2012). The development of the Nile drainage system: Integration of onshore and offshore evidence. Petroleum Geoscience, 18(4), 417–431. https://doi.org/10.1144/petgeo2011-074

Moneron, J., Gvirtzman, Z., Karcz, Z., & Sagy, Y. (2024). Discovery of the Messinian Eratosthenes Canyon in the deep Levant Basin. Global and Planetary Change, 232, 104318. https://doi.org/10.1016/j.gloplacha.2023.104318

Morag, N., Avigad, D., Gerdes, A., & Abbo, A. (2021). Detrital zircon and rutile U–Pb, Hf isotopes and heavy mineral assemblages of Israeli Miocene sands: Fingerprinting the Arabian provenance of the Levant. Basin Research,. https://doi.org/https://doi.org/10.1111/bre.12544

Morag, N., Haviv, I., & Katzir, Y. (2016). From ocean depths to mountain tops: Uplift of the Troodos ophiolite (Cyprus) constrained by low-temperature thermochronology and geomorphic analysis. Tectonics, 35(3), 622–637. https://doi.org/10.1002/2015TC004069

Morag, N., Haviv, I., Eyal, M., Kohn, B. P., & Feinstein, S. (2019). Early flank uplift along the Suez Rift: Implications for the role of mantle plumes and the onset of the Dead Sea Transform. Earth and Planetary Science Letters, 516, 56–65. https://doi.org/https://doi.org/10.1016/j.epsl.2019.03.002

Moustafa, A. R. (2020). Mesozoic-Cenozoic Deformation History of Egypt. In Z. Hamimi, A. El-Barkooky, J. Martínez Frías, H. Fritz, & Y. Abd El-Rahman (Eds.), The Geology of Egypt (pp. 253–294). Springer International Publishing. https://doi.org/10.1007/978-3-030-15265-9_7

Moustafa, A. R., Salama, M. E., Khalil, S. M., & Fouda, H. G. A. (2014). Sinai hinge belt: a major crustal boundary in NE Africa. Journal of the Geological Society, 171(2), 239–254. https://doi.org/10.1144/jgs2013-021

Needham, D. L., Pettingill, H. S., Christensen, C. J., Ffrench, J., & Karcz, Z. K. (2017). The Tamar giant gas field: Opening the Subsalt Miocene gas play in the Levant Basin. In AAPG Memoir (Vol. 113, pp. 221–256). American Association of Petroleum Geologists. https://doi.org/10.1306/13572009M1133688

Nuriel, P., Weinberger, R., Kylander-Clark, A. R. C., Hacker, B. R., & Craddock, J. P. (2017). The onset of the Dead Sea transform based on calcite age-strain analyses. Geology, 45(7), 587–590. https://doi.org/10.1130/G38903.1

Oren, O., Nuriel, P., Kylander-Clark, A. R. C., & Haviv, I. (2020). Evolution and propagation of an active plate boundary: U-Pb ages of fault-related calcite from the Dead Sea Transform. Tectonics, 39, e2019TC005888. https://doi.org/10.1029/2019TC005888

Oren, O., Nuriel, P., Kylander-Clark, A. R. C., & Haviv, I. (2023) Deciphering the Africa-Arabia: Insights from U-Pb dating along the Carmel-Gilboa fault system and its triple junction with the Dead Sea transform. Earth and Planetary Science Letters, 611, 118152. https://doi.org/10.1016/j.epsl.2023.118152

Papadimitriou, N., Gorini, C., Nader, F. H., Deschamps, R., Symeou, V., & Lecomte, J. C. (2018). Tectono-stratigraphic evolution of the western margin of the Levant Basin (offshore Cyprus). Marine and Petroleum Geology, 91, 683–705. https://doi.org/10.1016/j.marpetgeo.2018.02.006

Robertson, A. (1998a). Mesozoic-Tertiary tectonic evolution of the easternmost Mediterranean area: Integration of marine and land evidence. Proceedings of the Ocean Drilling Program: Scientific Results, 160, 723–784. https://doi.org/10.2973/odp.proc.sr.160.061.1998

Robertson, Al. (1998b). Tectonic significance of the Eratosthenes Seamount: a continental fragment in the process of collision with a subduction zone in the eastern Mediterranean (Ocean Drilling Program Leg 160). Tectonophysics, 298, 63-82. https://doi.org./10.1016/S0040-1951(98)00178-4.

Robertson, A. (2007). Overview of tectonic settings related to the rifting and opening of Mesozoic ocean basins in the Eastern Tethys: Oman, Himalayas and Eastern Mediterranean regions. Geological Society, London, Special Publications, 282(1), 325. https://doi.org/10.1144/SP282.15

Rozenbaum, A. G., Sandler, A., Zilberman, E., Stein, M., Jicha, B. R., and Singer, B. S. (2014). ^{40}AR/^{39}AR chronostratigraphy of late Miocene – early Pliocene continental aquatic basins in SE Galilee, Israel. Geological Society of America Bulletin., 128, 1383-1402, https://doi.org/10.1130/B31239.1

Ryan, W. B. F. (2009). Decoding the mediterranean salinity crisis. Sedimentology, 56(1), 95–136. https://doi.org/10.1111/j.1365-3091.2008.01031.x

Sagy, Y., Gvirtzman, Z., & Reshef, M. (2018). 80 m.y. of folding migration: New perspective on the Syrian arc from Levant Basin analysis. Geology, 46(2), 175–178. https://doi.org/10.1130/G39654.1

Sagy, Y., Gvirtzman, Z., Reshef, M., & Makovsky, Y. (2015). The enigma of the Jonah high in the middle of the Levant basin and its significance to the history of rifting. Tectonophysics, 665, 186–198. https://doi.org/10.1016/j.tecto.2015.09.037

Sagy, Y., & Gvirtzman, Z. (2024). Interplay between early rifting, later folding, and sedimentary filling of a long-lived Tethys remnant: The Levant Basin. Earth-Science Reviews, 104768. https://doi.org/10.1016/j.earscirev.2024.104768

Segev, A., Lyakhovsky, V., & Weinberger, R. (2014). Continental transform-rift interaction adjacent to a continental margin: The Levant case study. Earth-Science Reviews, 139, 83–103. Elsevier. https://doi.org/10.1016/j.earscirev.2014.08.015

Schattner, U., Ben-Avraham, Z., Reshef, M., Bar-Am, G., & Lazar, M. (2006a). Oligocene-Miocene formation of the Haifa basin: Qishon-Sirhan rifting coeval with the Red Sea-Suez system, Tectonophysics, 419, 1-12.

Schattner, U., Ben-Avraham, Z., Reshef, M., Bar-Am, G., Lazar, M., and Hübscher, C. (2006b). Tectonic isolation of the Levant basin offshore Galilee-Lebanon effects of the Dead Sea fault plate boundary on the Levant continental margin, eastern Mediterranean, Journal of Structural Geology, 28, 2049-2066.

Schattner, U., Ben-Avraham, Z. (2007). Transform margin of the northern Levant, eastern Mediterranean: From formation to reactivation. Tectonics, 26, 5. https://doi.org/10.1029/2007TC002112

Segev, A., Lyakhovsky, V. and Weinberger, R. (2014). Continental transform-rift interaction adjacent to a continental margin: The Levant case study, Earth Sci., 139, 83-103.

Shaliv, G. (1991). Stages in the tectonic and volcanic history of the Neogene basin in the Lower Galilee and the valleys. Israel Geological Survey Reposts, GSI/11/91, 101.

Simmons, M. D., Sharland, P. R., Casey, D. M., Davies, R. B., & Sutcliffe, O. E. (2007). Arabian Plate sequence stratigraphy: Potential implications for global chronostratigraphy. GEOARABIA-MANAMA-, 12(4), 101.

Stockli, D.F., Bosworth, W. (2019). Timing of Extensional Faulting Along the Magma-Poor Central and Northern Red Sea Rift Margin—Transition from Regional Extension to Necking Along a Hyperextended Rifted Margin. In: Rasul, N., Stewart, I. (eds) Geological Setting, Palaeoenvironment and Archaeology of the Red Sea. Springer, Cham. https://doi-org.iclibezp1.cc.ic.ac.uk/10.1007/978-3-319-99408-6_5

Stearman, M., Gergurich, B., Kent, T., Wickard, A., & Laugier, F. (2021). Miocene Deep-Water Stratigraphic Architecture and Heterogeneity: Levant Basin, Offshore Cyprus and Israel. Third EAGE Eastern Mediterranean Workshop, 2021(1), 1–3. https://doi.org/10.3997/2214-4609.202137034

Steinberg, J., Gvirtzman, Z., & Folkman, Y. (2010). New age constraints on the evolution of the Mt Carmel structure and its implications on a Late Miocene extensional phase of the Levant continental margin. Journal of the Geological Society, 167(1), 203-216. https://doi.org/10.1144/0016-76492009-089

Steinberg, J., Gvirtzman, Z., Folkman, Y., & Garfunkel, Z. (2011). Origin and nature of the rapid late Tertiary filling of the Levant Basin. Geology, 39(4), 355–358. https://doi.org/10.1130/G31615.1

Steinberg, J. (2012), The Rapid Sedimentary Filling of the Levant Basin Alongside the Arabian-African Breakup and the Relationship to the Deformation of its Margins, 149 pp., Geological Survey of Israel, Jerusalem. GSI/39/2012

Steinberg, J., Roberts, A. M., Kusznir, N. J., Schafer, K., & Karcz, Z. (2018). Crustal structure and post-rift evolution of the Levant Basin. Marine and Petroleum Geology, 96, 522–543. https://doi.org/10.1016/j.marpetgeo.2018.05.006

Stow, D.A.V., Howell, D.G., Nelson C. (1985). Sedimentary, tectonic and seal-level controls. In: Bouma, A.H, Normark, W.R., Barnes, N.E. (Eds.), Submarine Fans and Related Turbidie Ststems. Springer, New York, 215-222. https://doi.org/10.1007/978-1-4612-5114-9_4

Tillmans, F., Gawthorpe, R. L., Jackson, C. A. L., & Rotevatn, A. (2021). Syn-rift sediment gravity flow deposition on a Late Jurassic fault-terraced slope, northern North Sea. *Basin Research*, *33*(3), 1844-1879. https://doi.org/10.1111/bre.12538

Torfstein, A., & Steinberg, J. (2020). The Oligo–Miocene closure of the Tethys Ocean and evolution of the proto-Mediterranean Sea. Scientific Reports, 10(1), 13817. https://doi.org/10.1038/s41598-020-70652-4.

Wald, R., Segev, A., Ben-Avraham, Z., & Schattner, U. (2019). Structural expression of a fading rift front: a case study from the Oligo-Miocene Irbid rift of northwest Arabia. Solid Earth, 10, 225-250.

Weinberger, R., Nuriel, P., Kylander-Clark, A. R. C., & Craddock, J. P. (2020). Temporal and spatial relations between large-scale fault systems: Evidence from the Sinai-Negev shear zone and the Dead Sea Fault. Earth-Science Reviews, 211, 103377. https://doi.org/10.1016/j.earscirev.2020.103377

Zachos, J., Pagani, M., Sloan, L., Thomas, E., & Billups, K. (2001). Trends, rhythms, and aberrations in global climate 65 Ma to present. science, 292(5517), 686-693. https://doi.org/10.1126/science.1059412

Ziegler, A. M. (2001). Late Permian to Holocene Paleofacies Evolution of the Arabian Plate and its Hydrocarbon Occurrences. GeoArabia, 6(3), 445–504.

Zilberman, E., & Calvo, R. (2013). Remnants of Miocene fluvial sediments in the Negev Desert, Israel, and the Jordanian Plateau: Evidence for an extensive subsiding basin in the northwestern margins of the Arabian plate. Journal of African Earth Sciences, 82, 33–53. https://doi.org/https://doi.org/10.1016/j.jafrearsci.2013.02.006

Table Captions

Table 1: Summary of the main geophysical data of the seismic reflection surveys used.

Tables

Table 1

Name	Leviathan	Sara-Mira-Arie	Shimshon-Daniel	Royee	smasDI_019	TGS
Type	3D	3D	3D	3D	2D	2D
Area (Km^2)	2,355	1,750	1,410	512	NA	
Total line length (km)	NA				943	880
Acquisition year	2010	2009 (Sara-Mira) 2012 (Arie)	2014	2010	2001	2001
Reprocessed	2019	2021	2021	NA	2021	2020
Final Bin size (m)	25x25	25x12.5	25x12.5	25x25	NA	
Vert. Res. (m)	50	45	40	50	NA	NA
Migration	PSDM					

Figure Captions

Figure 1: Regional map of the Levant Basin. Highlighted are the main morpho-structural elements in and around the basin. Insert indicate the different 3D surveys used for this study. The bathymetric metadata and Digital Terrain Model data products have been derived from EMODnet Bathymetry portal – https://www.emodnet-bathymetry.eu.

Figure 2: Top – Structural map of the Jonah High showing the triangular shape of this unique structure. Black line shows the outline of the Sara – Myra – Arie 3D survey, for location see insert in Figure 1. Bottom – Cross-sections through the structure, showing the onlaps of the Oligocene – Miocene strata. The structure was finally buried during the Langhian.

Figure 3: Synthesis of the main tectono-stratigraphic events which influenced on the development of the Levant Basin. Numbers next to each event are for the following references: [1] Torfstein and Steinberg (2020); [2] Buchbinder et al. (2005); [3] Gardosh et al. (2008a); [4] Hsü et al. (1977); [5] Zachos et al. (2001); [6] Bosworth et al. (2015); [7] Gvirtzman & Steinberg (2012); [8] Bar et al. 2016; [9[Bialik et al. (2019); [10] Bosworth et al. (2005); [11] Robertson et al. (1998); [12] Ziegler et al. (2001); [13] Sagy et al. (2018); [14] Needham et al. (2017); [15] Garfunkel et al. (1998); [16] Robertson et al. (2007); [17] Gao et al. (2020); [18] Nuriel et al. (2017); [19] Simmons et al. (2007); [20] Druckman et al. (1995); [21] Avni et al. (2012); [22] Faccenna et al. (2019); [23] Macgregor (2012); [24] Moustafa et al. (2014); [25] Weinberger et al. (2020); [26] Morag et al. (2019); [27] Stockli & Bosworth (2019); [28] Calvo & Barotv (2001); [29] Zilberman & Calvo (2013); [30] Glazer et al. (2023); [31] Oren et al. (2020); [32] Wald et al. (2019); [33] Joffe et al. (2022); [34] Shaliv (1991); [35] Oren et al. (2023).

Figure 4: (A) Thickness map of the Oligocene – Early Miocene (Aquitanian) seismic interval is generally isopachous, with a southerly depocenter and thinning above an anticline on the eastern side of the dataset. (B) Separation of the interval into two sub-units (i.e., left – Late Oligocene; right - Early Oligocene), show the anticline on the eastern side of the study area was only active in the Early Oligocene.

Figure 5: (A) Spectral decomposition extract from Late Oligocene – Early Miocene (Aquitanian) showing a system of dense turbidity-like features. (B) Spectral decomposition extract from Early Oligocene (Rupelian) showing wider, less sinuous features, trending more N-S. For additional extraction please see SP2 – 22

Figure 6: (A) Thickness map of the Early Burdigalian show initial thickness changes after a period of relative isopachous deposition. Thinning trends are seen towards the LTK-fault and east of Jonah High. (B) Spectral decomposition extract from the Early Burdigalian showing NE-trending channels alongside NR-trending fan-like features. For additional extraction please see SP23 – 27.

Figure 7: Spectral decomposition extract from the prominent valley-fill complex located at the southern end of the study area. The complex is bounded between the Early Burdigalian and the Early Tortonian intervals.

Figure 8: (A) Thickness map of the Late Burdigalian show regionally pervasive thickness changes associated with the NW-SE-striking normal faults. Additional prominent changes are thinning across the Leviathan High, adjacent to the LTK fault. (B) Spectral decomposition extract from the Late Burdigalian showing onlaps and stacking patterns on the eastern side of the study area. An additional northerly splay is also highlighted, as well as en-echelon like pattern on the south-west side of the study area. For additional extraction please see SP 28-32.

Figure 9: Cross-sections through the strike-slip system located in the Levant Basin. Cross section locations are indicated in (A). All cross-sections show a deep-rooted stem which splays upwards, like the strike-slip indicative negative flower structure.

Figure 10: (A) Langhian thickness map shows that across-fault thickness changes are only seen in the northern side of the study area. Thinning above the Leviathan High is now dome-like, unlike the LTK-related as seen in the Late Burdigalian (Figure 8). (B) Spectral decomposition extract and cross-sections show a bright, wide erosional surface, filled with onlapped younger strata. For additional extractions please see SP 33-40.

Figure 11: (A) Early Tortonian thickness map shows a general E – NE thinning trend The Jonah High is now completely covered, with its distinct triangular shape clearly present. (B) The chaotic seismic response of the Early Tortonian is transitioning into a continuous, layered reflections towards the NNW, where some NW-trending channels are well imaged. For additional extractions please see SP 41-45.

Figure 12: (A) Late Tortonian thickness map is mainly controlled by post-deposition incised valleys flowing NW. A general thinning trend is seen above the Leviathan High, with mild thinning also seen above the LTK fault. (B) Spectral decomposition, supported by cross-

sections, showing the different erosional valleys controlling the Late Tortonian stratigraphy. For additional extractions please see SP 46-49.

Figure 13: Synthesis of the Oligocene – Early Miocene tectono-stratigraphic events occurring in and around the Levant Basin. Early Oligocene was mainly controlled by Arabian source, whereas Late Oligocene and Early Miocene were mainly fed from an African source, once the Nile River started to develop in conjunction with the rise of the Red-Sea mountains.

Figure 14: Synthesis of the Early Burdigalian tectono-stratigraphic events occurring in and around the Levant Basin. Significant subsidence along the Azraq-Sirhan rift, alongside incision along the Afiq canyon and the deep-water sedimentology architecture indicate an Arabian source. Folding was initiated adjacent the LTK fault offshore, concurrent to folding occurring onshore Sinai and the activation of the Negev-Sinai Shear Zone and the nucleation of the Dead-Sea transform.

Figure 15: Synthesis of Late Burdigalian tectono-stratigraphic events occurring in and around the Levant Basin. Highlighted are the active NW-Se-striking normal faults nucleating onshore Sinai and across the Levant Basin. The offshore strike-slip fault networks are also highlighted and are believed to be related to the same event which nucleated the regional normal faulting and the northward propagation of the Dead-Sea transform. Also highlighted are the renewed incised valley canyons offshore (Green – Afiq, Blue – Ashdod and other regional transport system)

Figure 16: Synthesis of Langhian tectono-stratigraphic elements active in and around the Levant Basin. Highlighted are the location of the offshore extension of the Afiq Canyon, the Ziqlag formation, and the syn-depositional faulting occurring on the northern part of the study-area.

Figure 17: Synthesis of Tortonian tectono-stratigraphic elements active in and around the Levant Basin. Highlighted are the activation of the Carmel Fault, the subsidence along the Dead-Sea transform and the Late Tortonian vast NE-trending offshore incised valleys. North-directed Early Tortonian channels are marked in Brown.

Figures

Figure 1

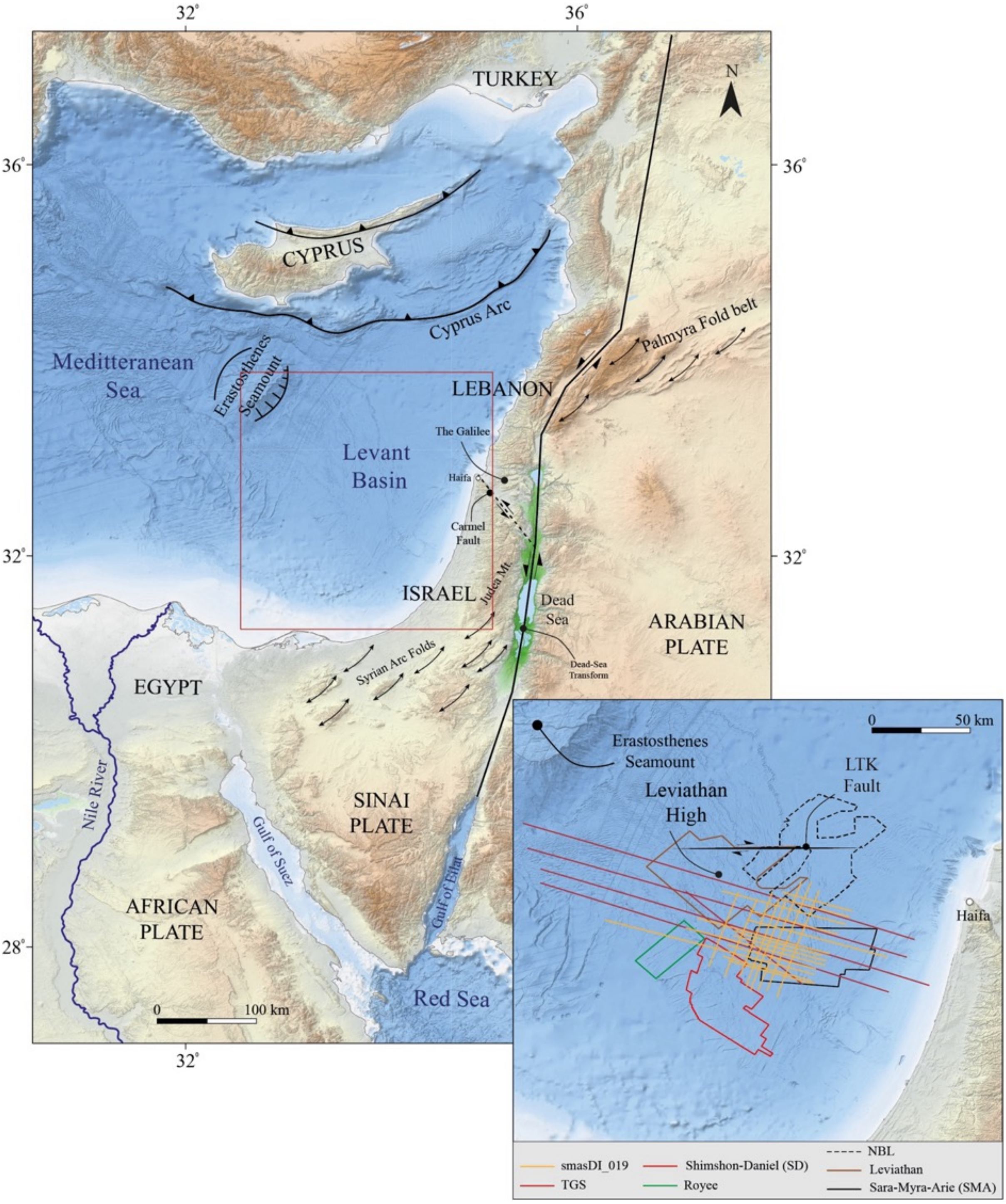

Figure 2

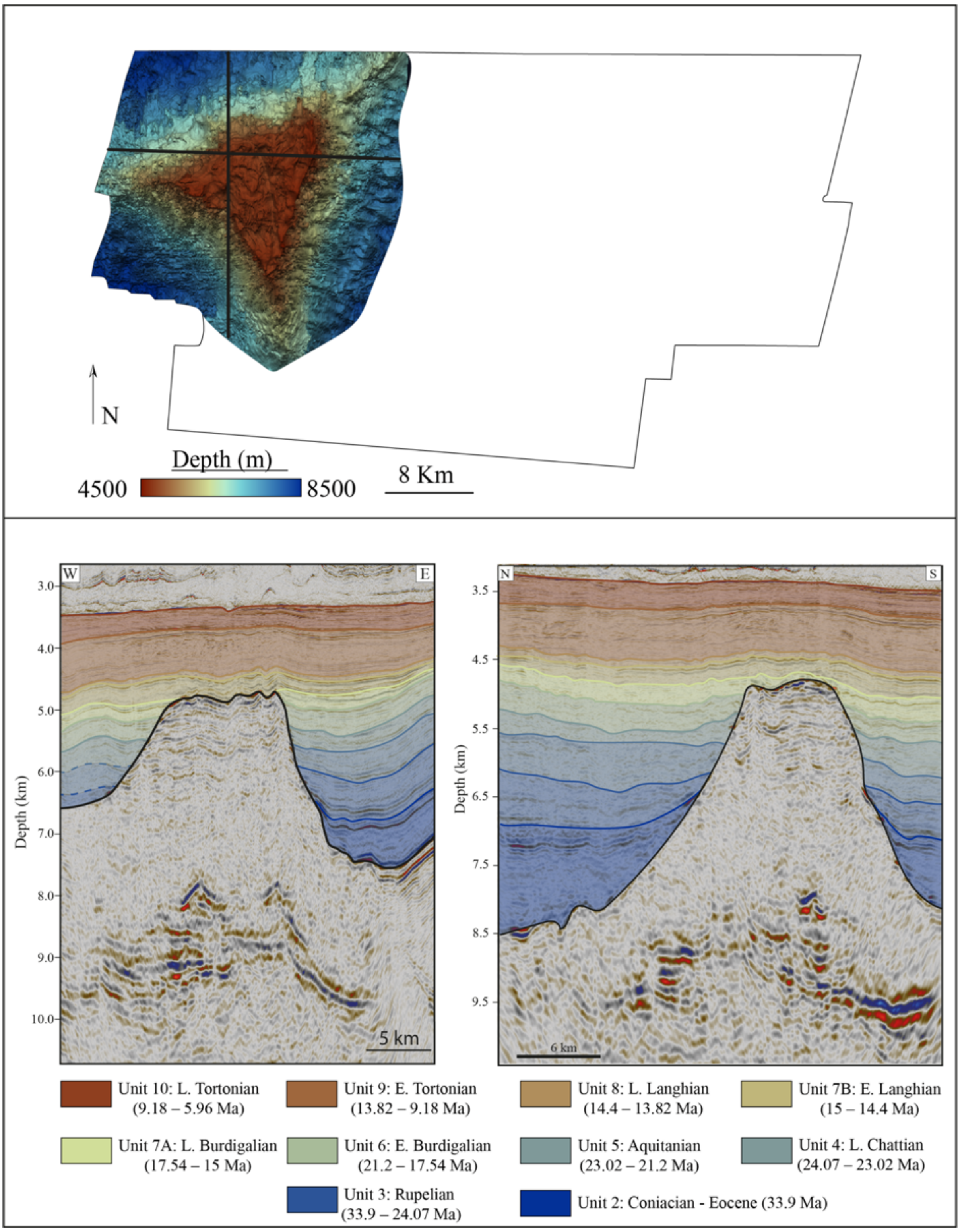
N
Depth (m)
4500
8500
8 Km
W
E
Depth (km)
3.0
4.0
5.0
6.0
7.0
8.0
9.0
10.0
5 km
N
S
3.5
4.5
5.5
6.5
7.5
8.5
9.5
6 km
Unit 10: L. Tortonian (9.18 – 5.96 Ma)
Unit 9: E. Tortonian (13.82 – 9.18 Ma)
Unit 8: L. Langhian (14.4 – 13.82 Ma)
Unit 7B: E. Langhian (15 – 14.4 Ma)
Unit 7A: L. Burdigalian (17.54 – 15 Ma)
Unit 6: E. Burdigalian (21.2 – 17.54 Ma)
Unit 5: Aquitanian (23.02 – 21.2 Ma)
Unit 4: L. Chattian (24.07 – 23.02 Ma)
Unit 3: Rupelian (33.9 – 24.07 Ma)
Unit 2: Coniacian - Eocene (33.9 Ma)

Figure 3

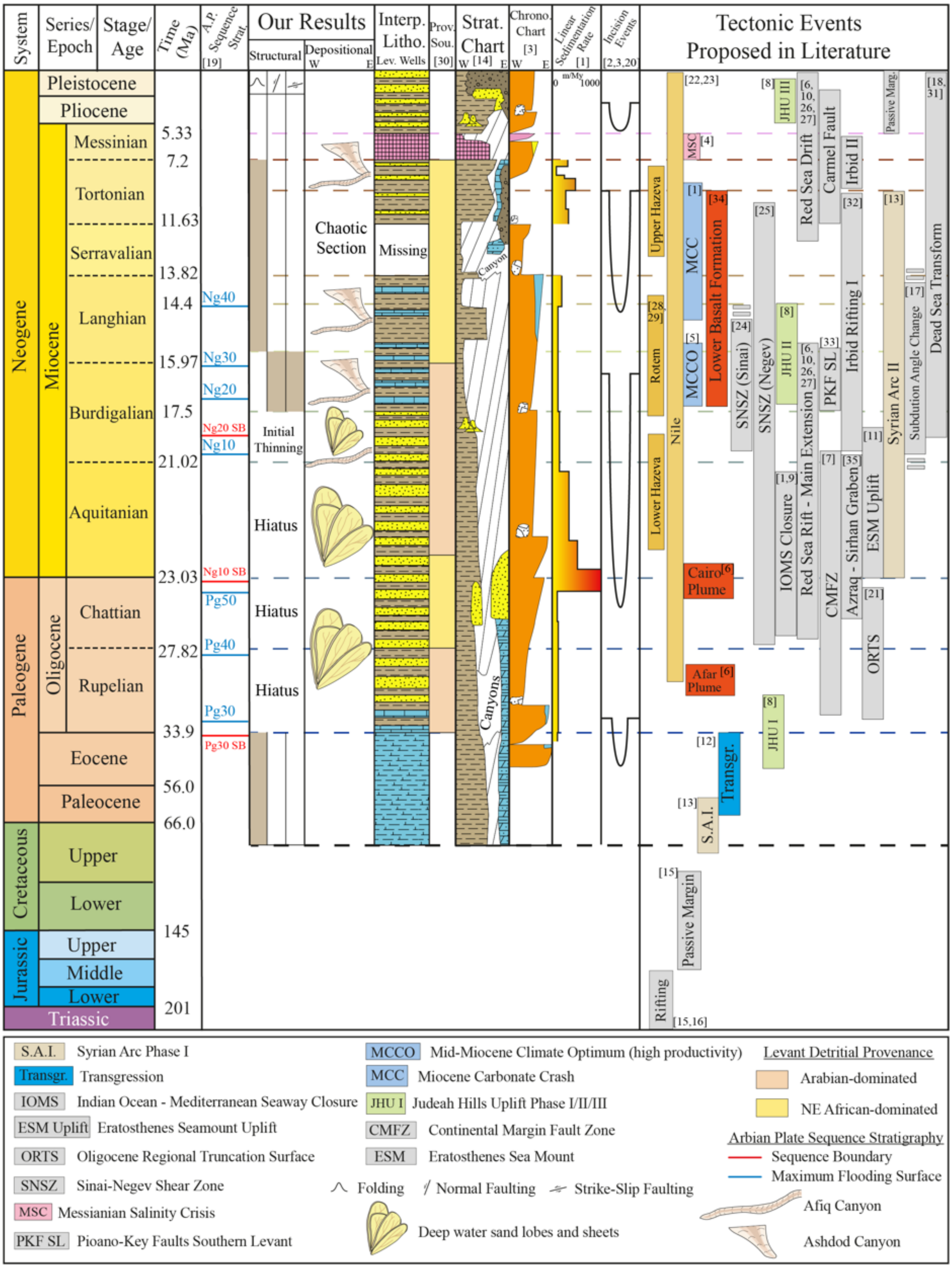

System
Series/ Epoch
Stage/ Age
Time (Ma)
A.P. Sequence Strat. [19]
Our Results
Structural
Depositional W E
Interp. Litho. Lev. Wells
Prov. Sou. [30]
Strat. Chart W [14] E
Chrono. Chart [3] W E
Linear Sedimentation Rate [1]
m/My
0
1000
Incision Events [2,3,20]
Tectonic Events Proposed in Literature
Neogene
Paleogene
Cretaceous
Jurassic
Triassic
Pleistocene
Pliocene
Miocene
Oligocene
Messinian
Tortonian
Serravalian
Langhian
Burdigalian
Aquitanian
Chattian
Rupelian
Eocene
Paleocene
Upper
Lower
Upper
Middle
Lower
5.33
7.2
11.63
13.82
14.4
15.97
17.5
21.02
23.03
27.82
33.9
56.0
66.0
145
201
Ng40
Ng30
Ng20
Ng20 SB
Ng10
Ng10 SB
Pg50
Pg40
Pg30
Pg30 SB
Chaotic Section
Initial Thinning
Hiatus
Hiatus
Hiatus
Missing
Canyon
Canyons
Upper Hazeva
Rotem
Lower Hazeva
Nile
MSC
MCC
MCCO
Lower Basalt Formation
Cairo Plume
Afar Plume
Transgr.
S.A.I.
Passive Margin
Rifting
SNSZ (Sinai)
SNSZ (Negev)
IOMS Closure
JHU III
JHU II
JHU I
Red Sea Drift
Red Sea Rift - Main Extension
Carmel Fault
PKF SL
CMFZ
Irbid II
Irbid Rifting I
Azraq - Sirhan Graben
ESM Uplift
ORTS
Passive Marg.
Syrian Arc II
Subdution Angle Change
Dead Sea Transform
[22,23]
[8]
[6, 10, 26, 27]
[4]
[1]
[34]
[25]
[32]
[13]
[28, 29]
[24]
[8]
[5]
[17]
[33]
[6, 10, 26, 27]
[11]
[1,9]
[7]
[35]
[21]
[8]
[12]
[13]
[15]
[15,16]
[18, 31]
[6]
[6]
S.A.I. Syrian Arc Phase I
Transgr. Transgression
IOMS Indian Ocean - Mediterranean Seaway Closure
ESM Uplift Eratosthenes Seamount Uplift
ORTS Oligocene Regional Truncation Surface
SNSZ Sinai-Negev Shear Zone
MSC Messinian Salinity Crisis
PKF SL Pioano-Key Faults Southern Levant
MCCO Mid-Miocene Climate Optimum (high productivity)
MCC Miocene Carbonate Crash
JHU I Judeah Hills Uplift Phase I/II/III
CMFZ Continental Margin Fault Zone
ESM Eratosthenes Sea Mount
Folding
Normal Faulting
Strike-Slip Faulting
Deep water sand lobes and sheets
Levant Detritial Provenance
Arabian-dominated
NE African-dominated
Arbian Plate Sequence Stratigraphy
Sequence Boundary
Maximum Flooding Surface
Afiq Canyon
Ashdod Canyon

Figure 4

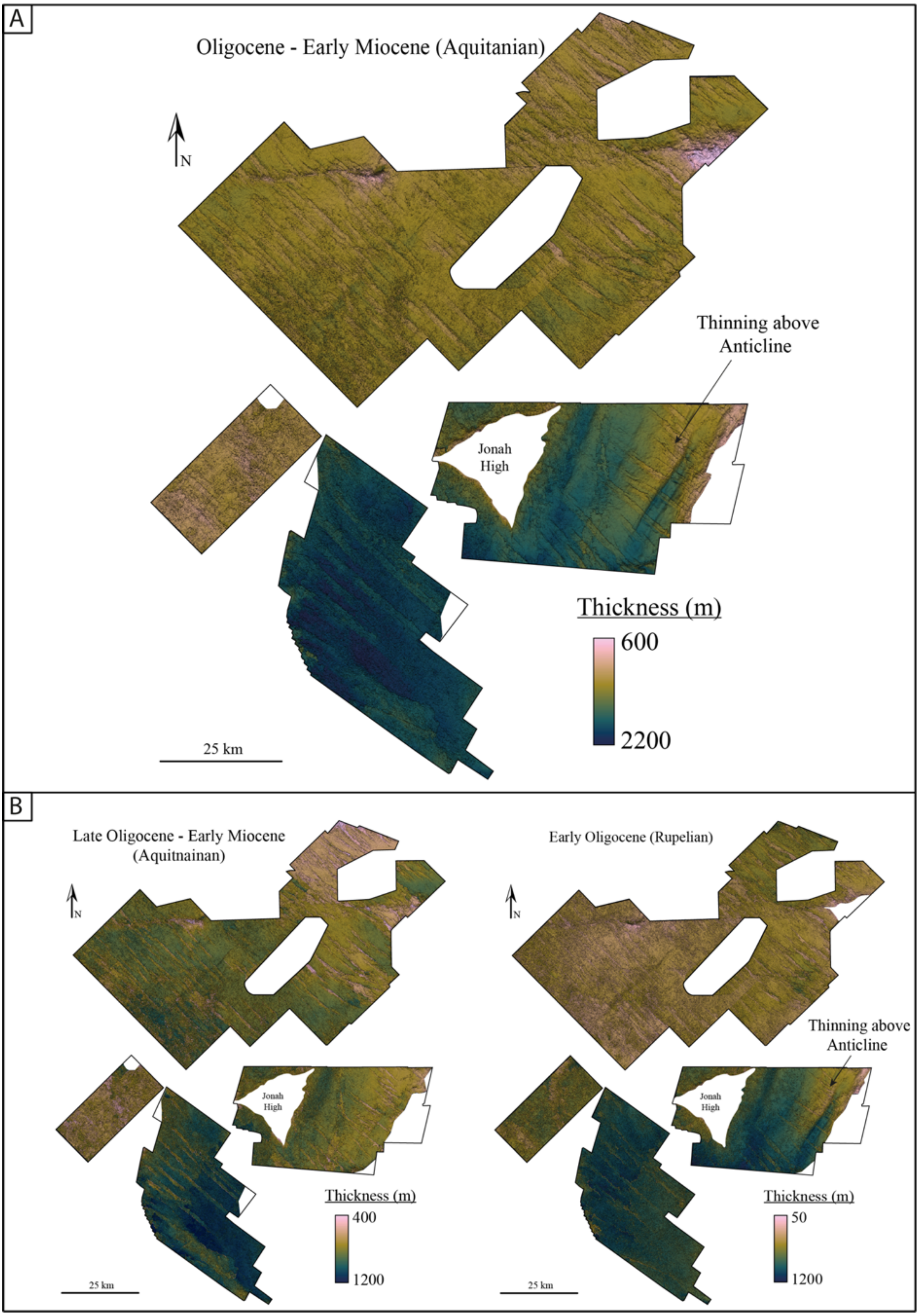
A
Oligocene - Early Miocene (Aquitanian)
N
Thinning above Anticline
Jonah High
Thickness (m)
600
2200
25 km
B
Late Oligocene - Early Miocene (Aquitnainan)
N
Jonah High
Thickness (m)
400
1200
25 km
Early Oligocene (Rupelian)
N
Thinning above Anticline
Jonah High
Thickness (m)
50
1200
25 km

Figure 5

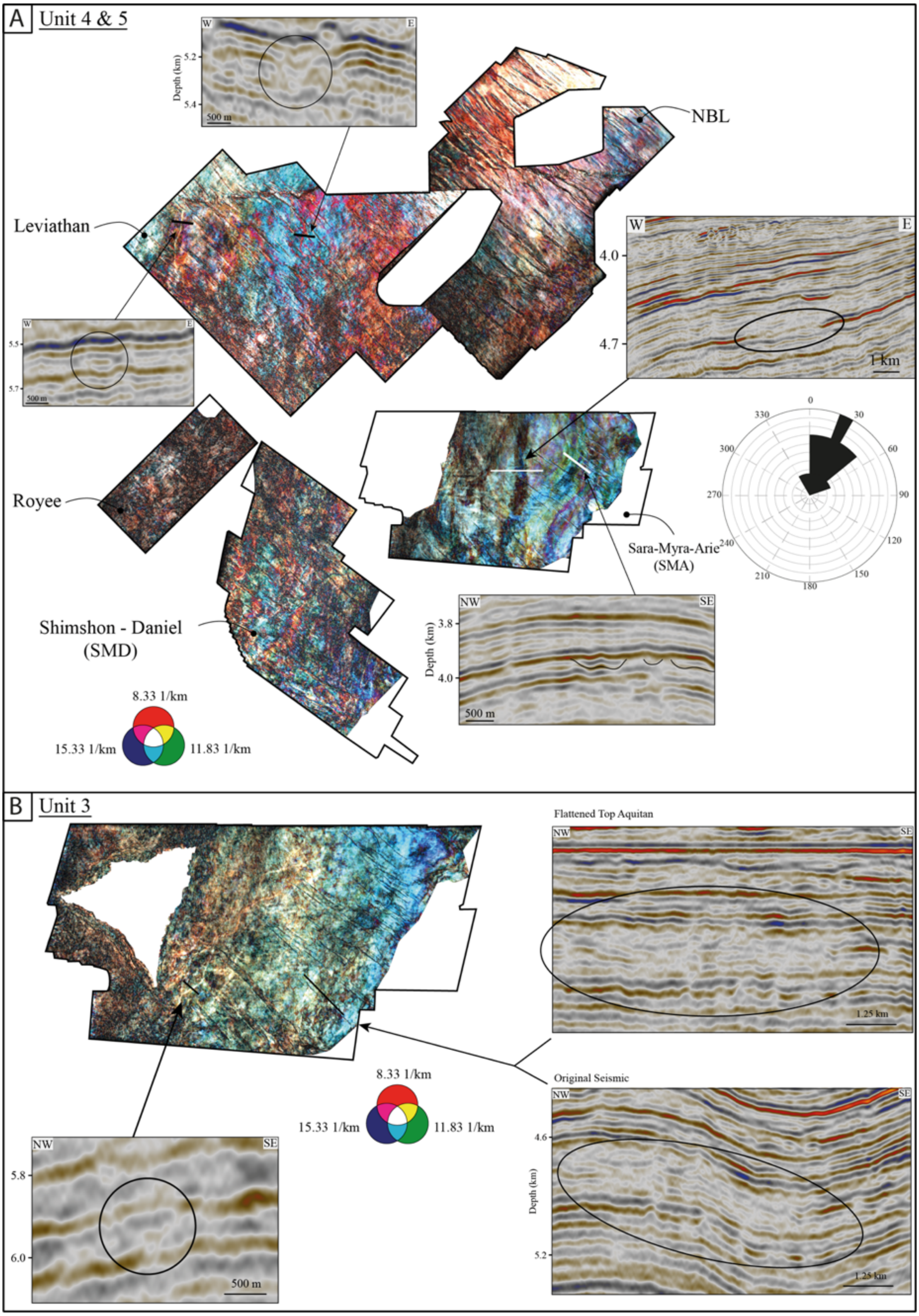

A
Unit 4 & 5
W
E
Depth (km)
5.2
5.4
500 m
NBL
Leviathan
W
E
4.0
4.7
1 km
5.5
5.7
500 m
Royee
0
30
60
90
120
150
180
210
240
270
300
330
Sara-Myra-Arie
(SMA)
Shimshon - Daniel
(SMD)
NW
SE
3.8
4.0
Depth (km)
500 m
8.33 1/km
15.33 1/km
11.83 1/km
B
Unit 3
Flattened Top Aquitan
NW
SE
1.25 km
Original Seismic
NW
SE
4.6
5.2
Depth (km)
1.25 km
8.33 1/km
15.33 1/km
11.83 1/km
NW
SE
5.8
6.0
500 m

1026 <u>Figure 6</u>

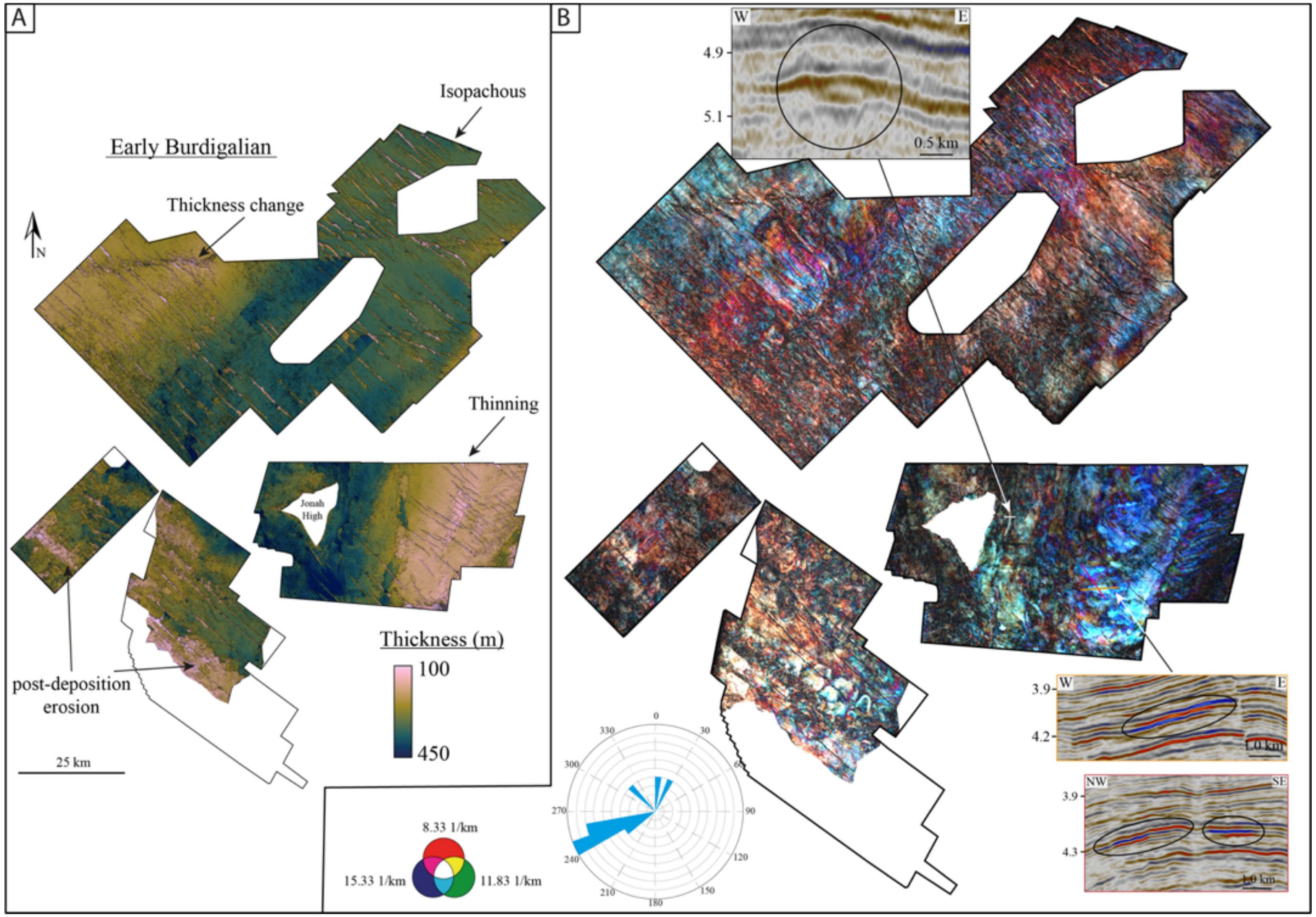

1027

1028

1029 <u>Figure 7</u>

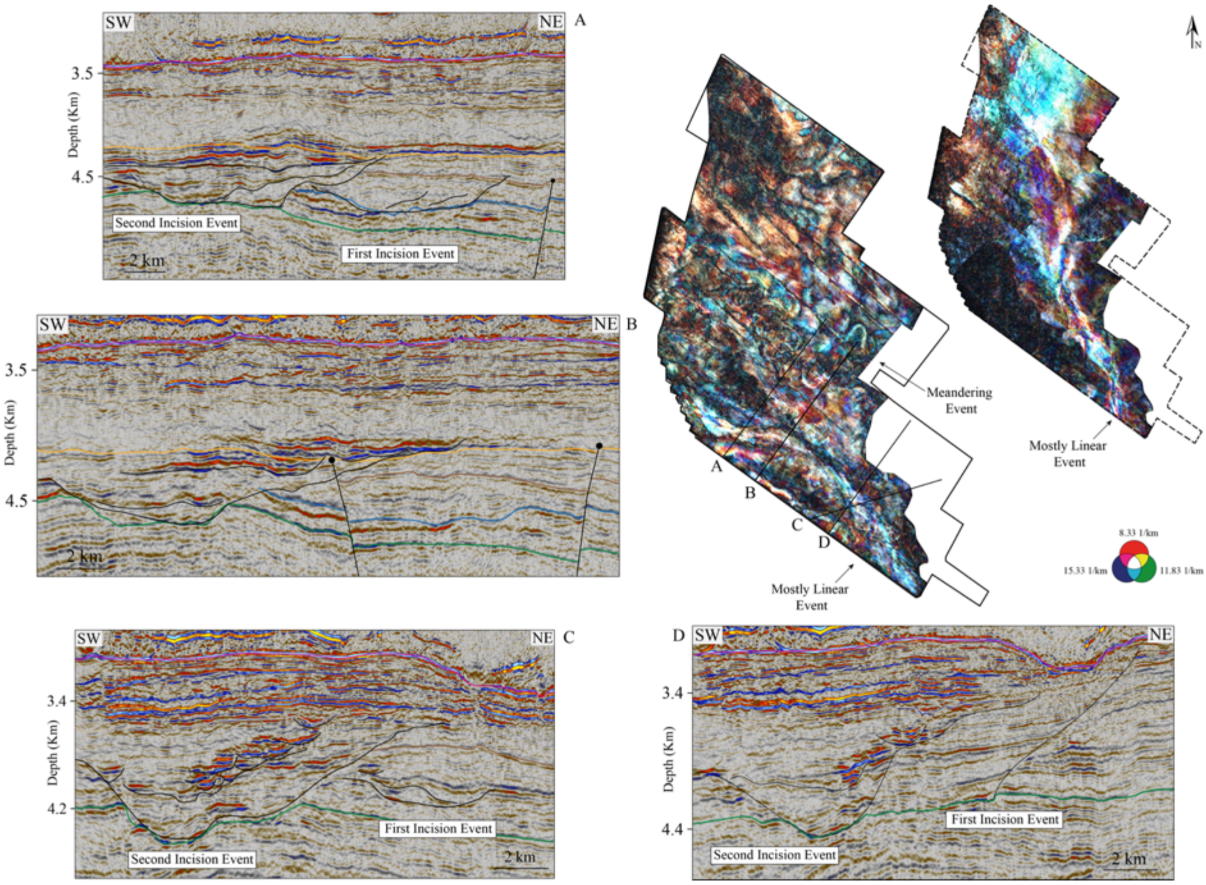

1030

1031

1032 Figure 8

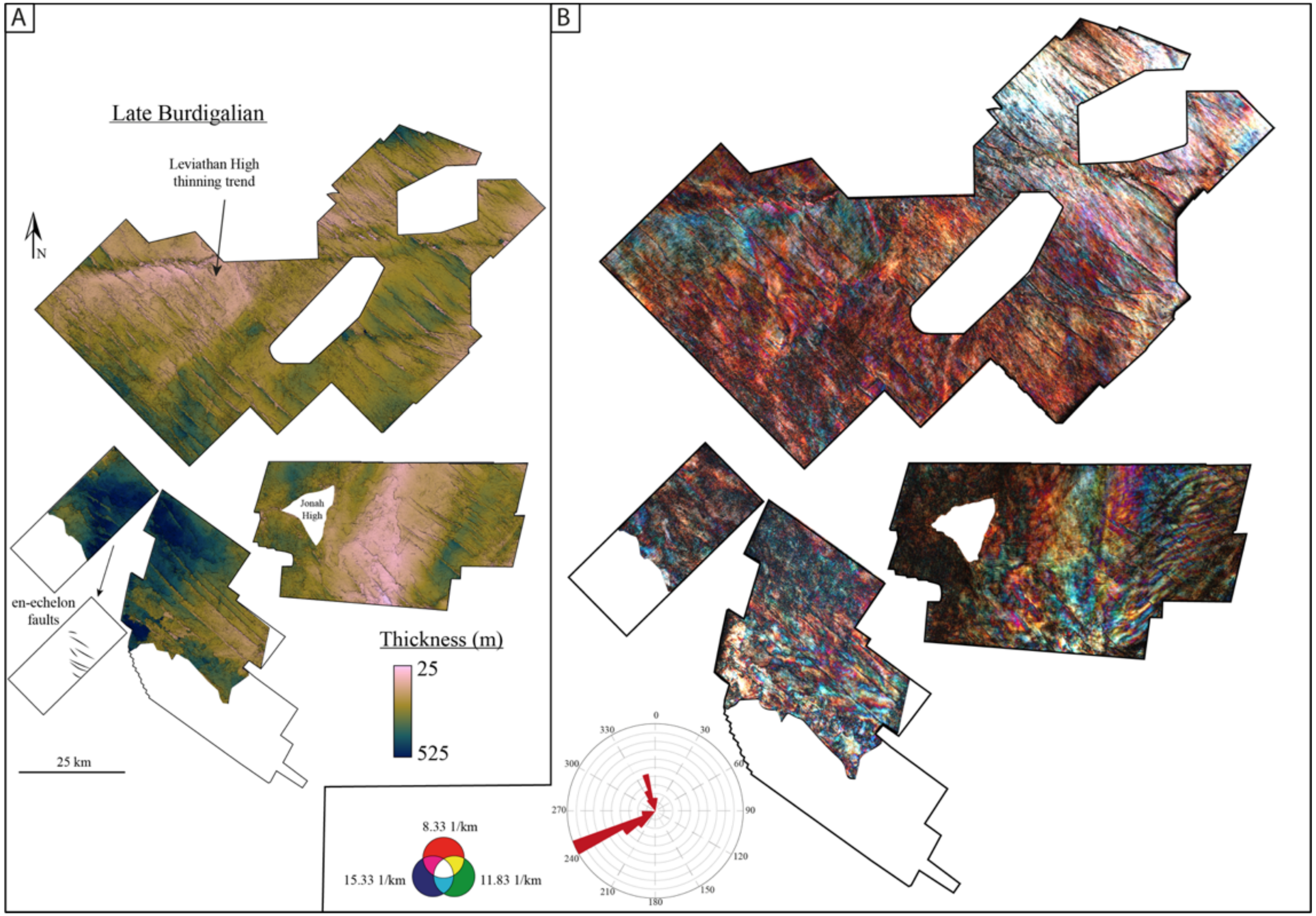

1033

1034

1035 Figure 9

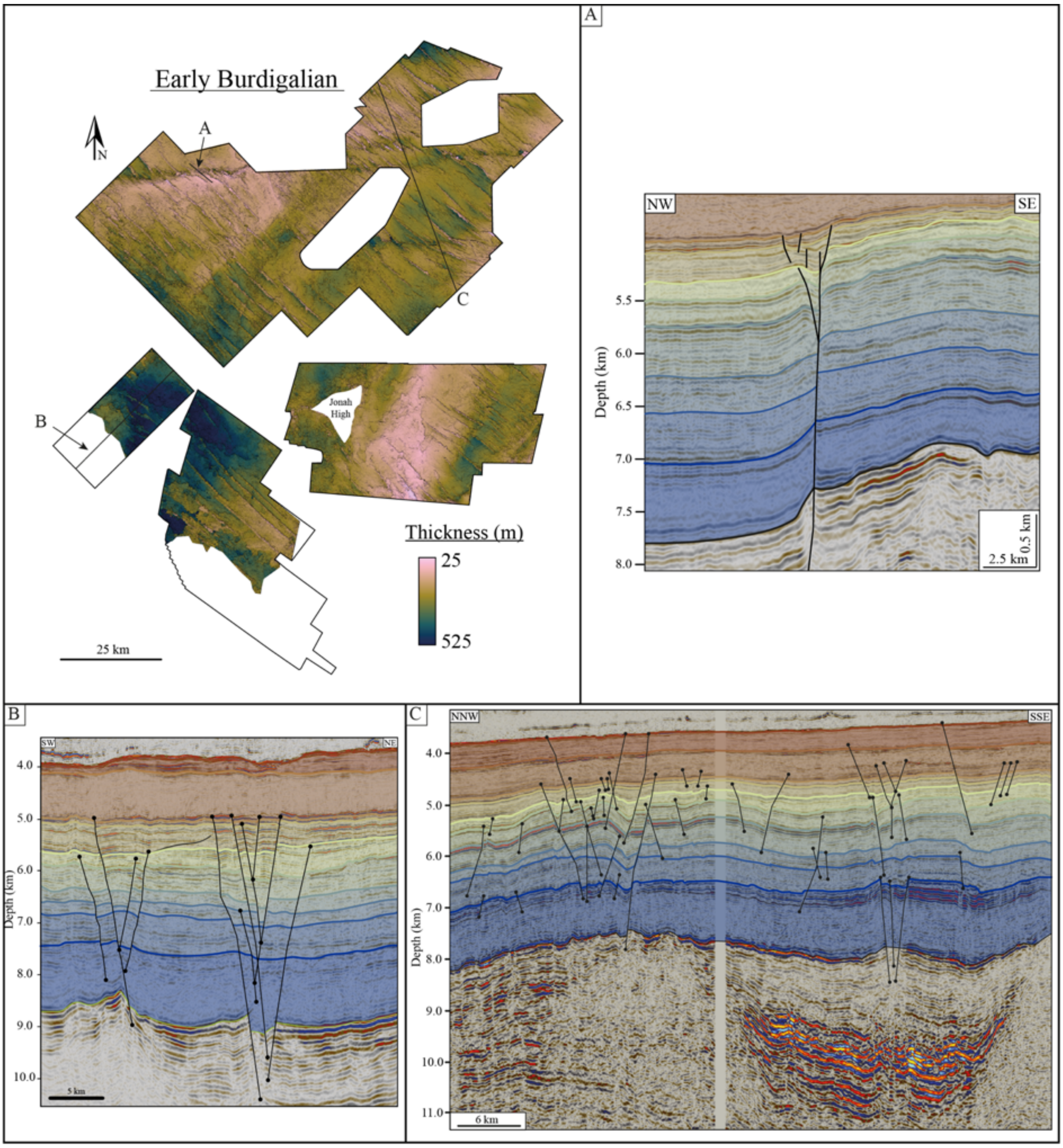

1036

1037

1038 Figure 10

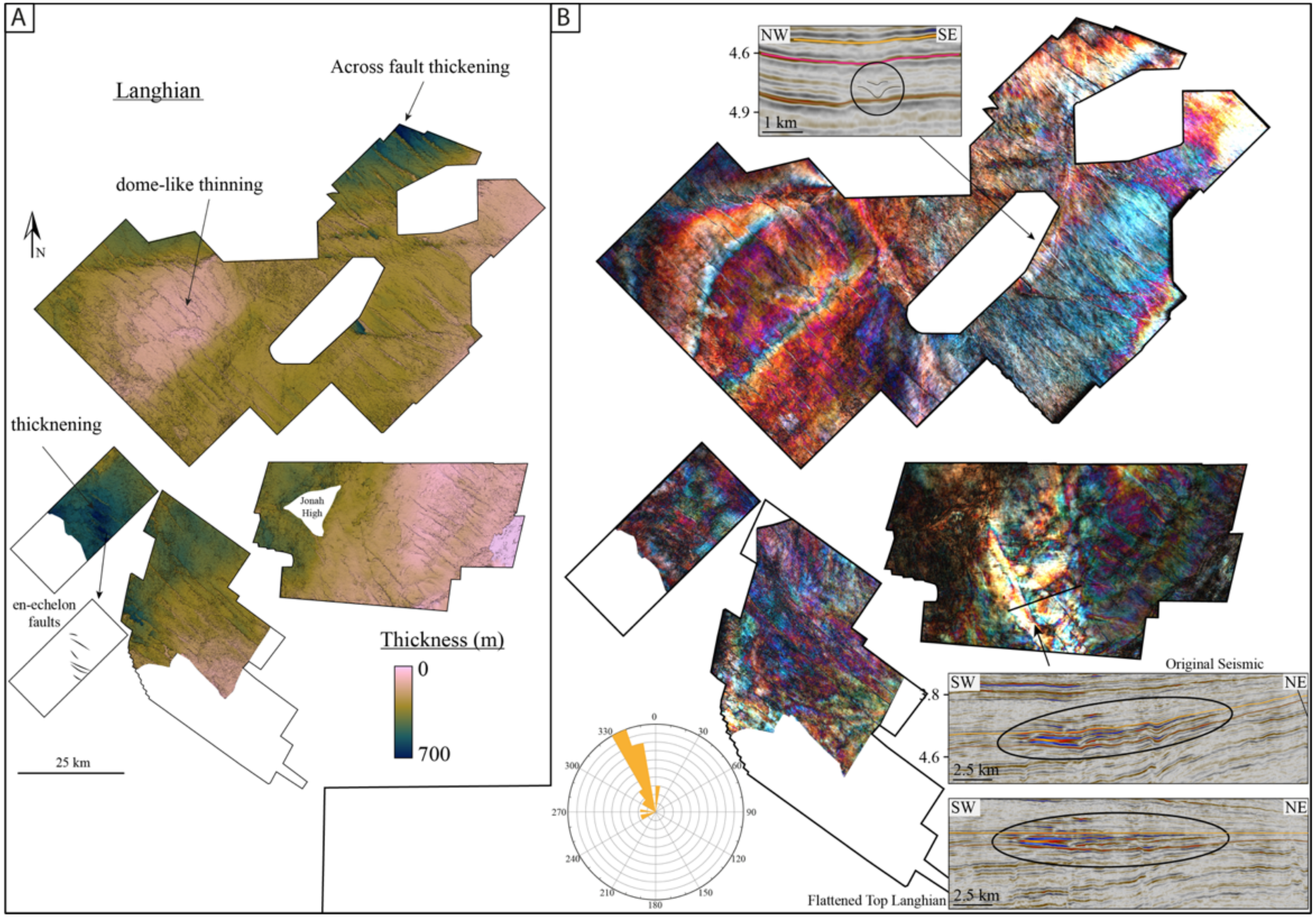

1039

1040

1041 Figure 11

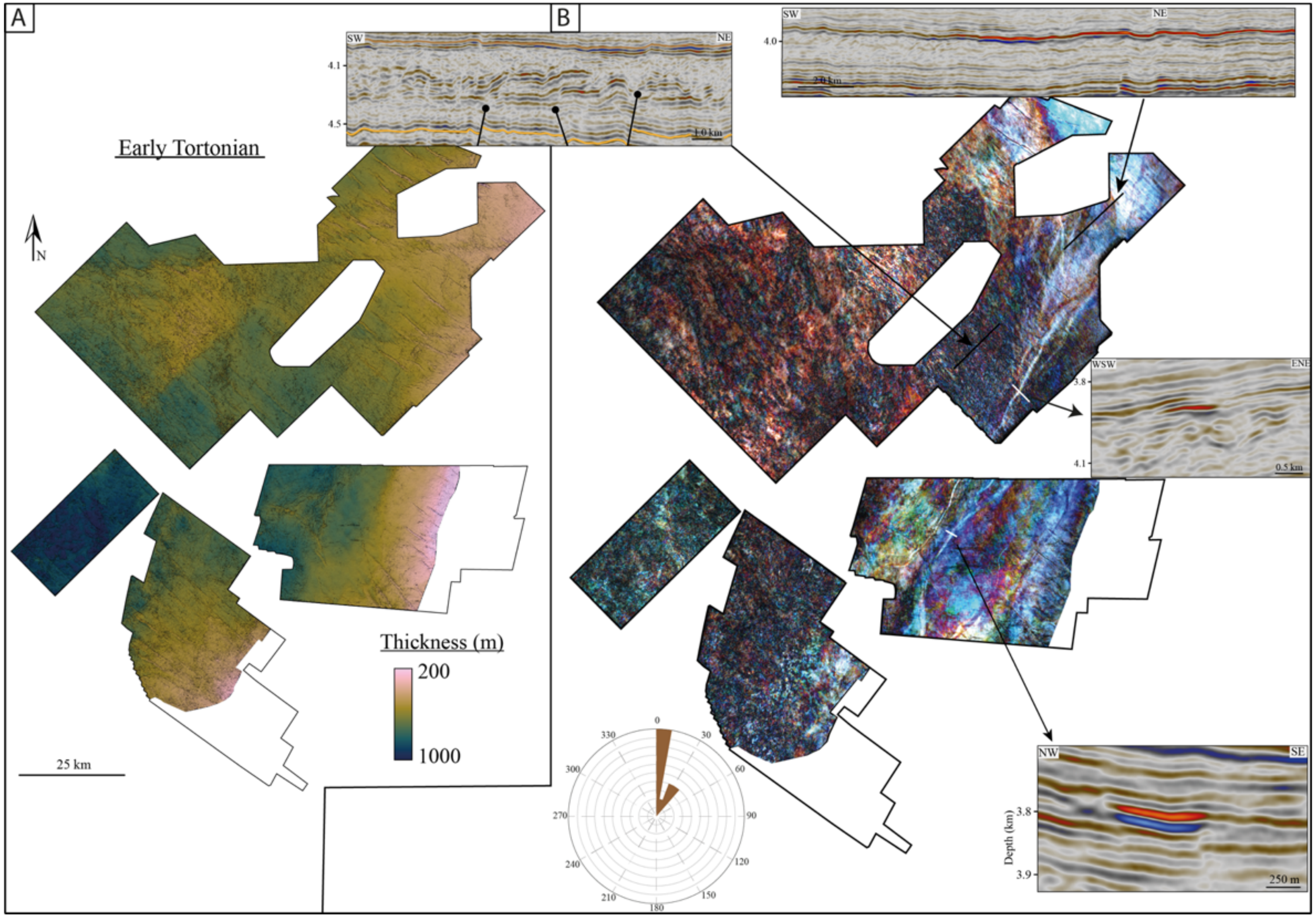

1042

1043

1044 Figure 12

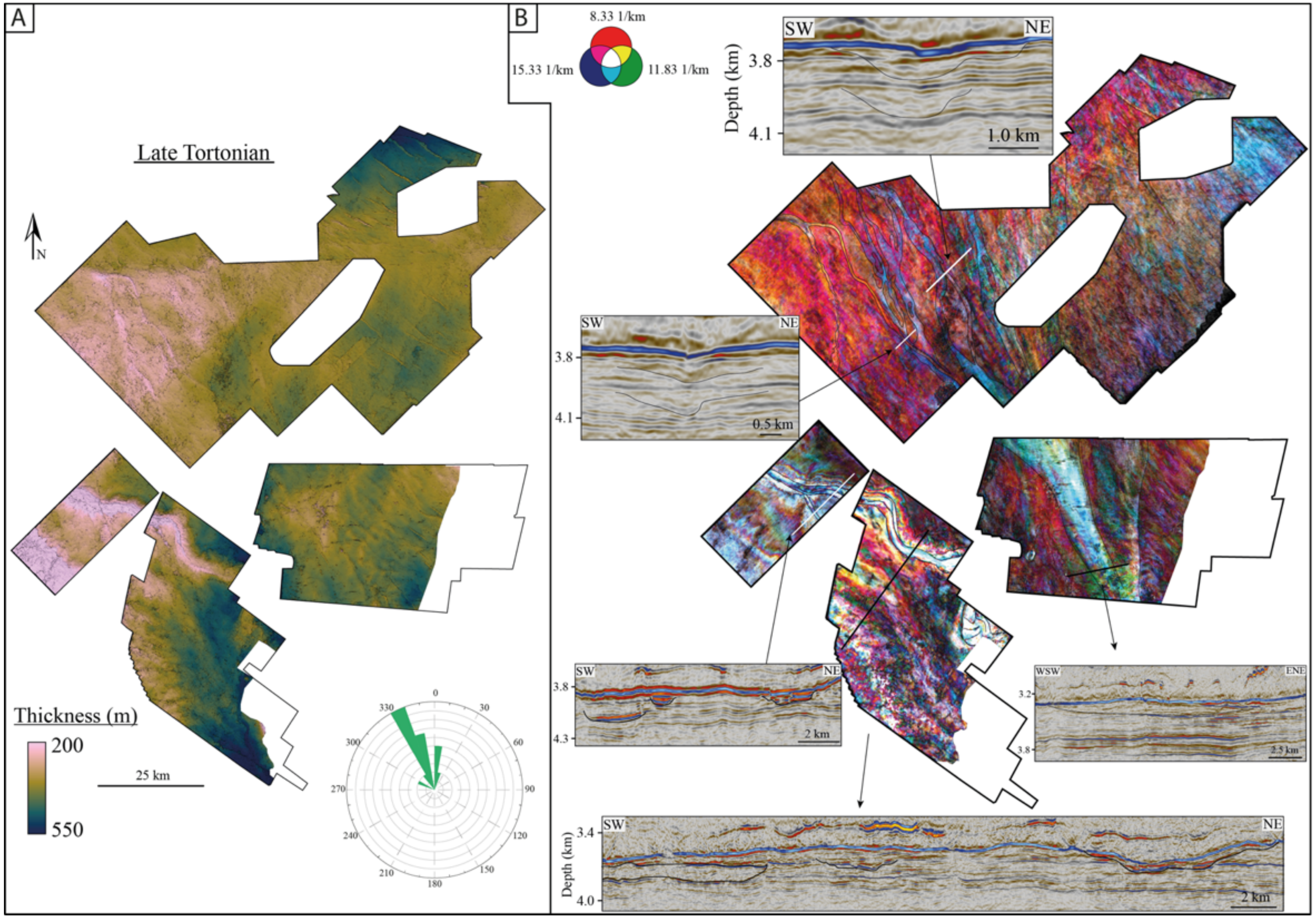

1045

1046

Figure 13

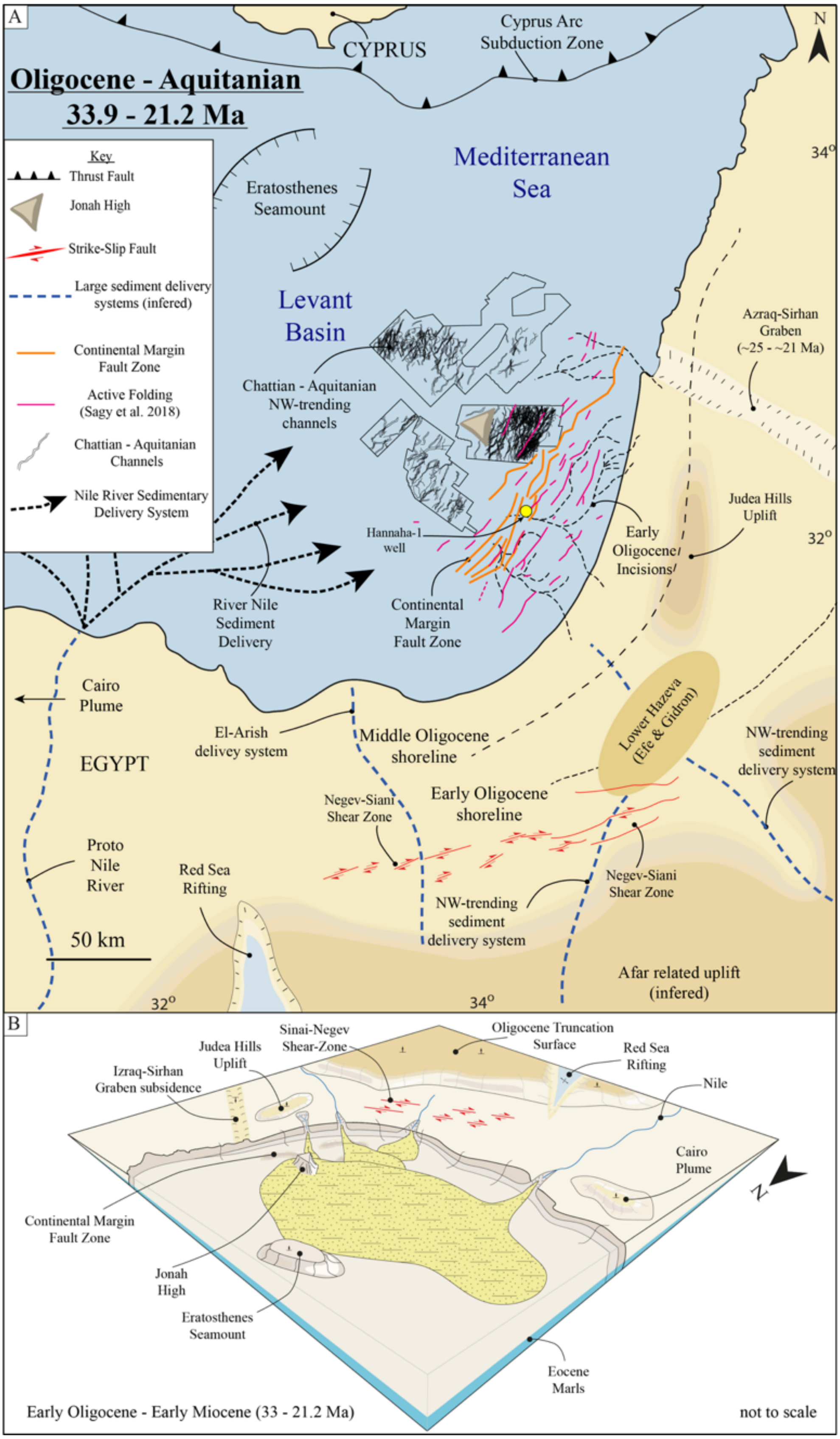

A
CYPRUS
Cyprus Arc
Subduction Zone
N
Oligocene - Aquitanian
33.9 - 21.2 Ma
Key
Thrust Fault
Jonah High
Strike-Slip Fault
Large sediment delivery systems (infered)
Continental Margin Fault Zone
Active Folding (Sagy et al. 2018)
Chattian - Aquitanian Channels
Nile River Sedimentary Delivery System
Eratosthenes
Seamount
Mediterranean
Sea
34°
Levant
Basin
Azraq-Sirhan
Graben
(~25 - ~21 Ma)
Chattian - Aquitanian
NW-trending
channels
Judea Hills
Uplift
32°
Hannaha-1
well
Early
Oligocene
Incisions
River Nile
Sediment
Delivery
Continental
Margin
Fault Zone
Cairo
Plume
El-Arish
delivey system
Middle Oligocene
shoreline
Lower Hazeva
(Efe & Gidron)
NW-trending
sediment
delivery system
EGYPT
Negev-Siani
Shear Zone
Early Oligocene
shoreline
Proto
Nile
River
Red Sea
Rifting
Negev-Siani
Shear Zone
NW-trending
sediment
delivery system
50 km
Afar related uplift
(infered)
32°
34°
B
Sinai-Negev
Shear-Zone
Oligocene Truncation
Surface
Judea Hills
Uplift
Red Sea
Rifting
Izraq-Sirhan
Graben subsidence
Nile
Cairo
Plume
N
Continental Margin
Fault Zone
Jonah
High
Eratosthenes
Seamount
Eocene
Marls
Early Oligocene - Early Miocene (33 - 21.2 Ma)
not to scale

Figure 14

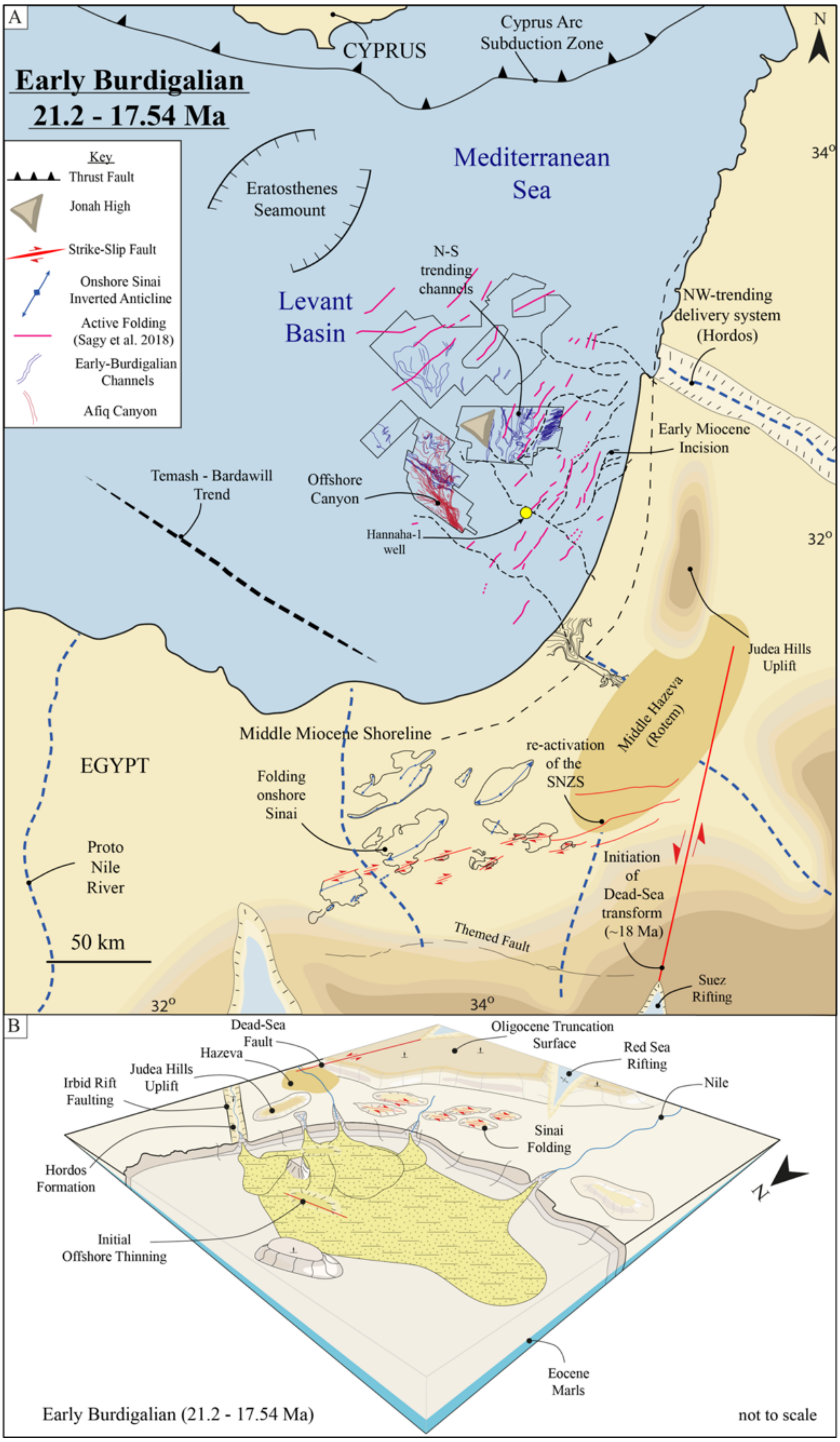

A
Early Burdigalian
21.2 - 17.54 Ma
CYPRUS
Cyprus Arc
Subduction Zone
N
34°
Mediterranean
Sea
Eratosthenes
Seamount
Key
Thrust Fault
Jonah High
Strike-Slip Fault
Onshore Sinai
Inverted Anticline
Active Folding
(Sagy et al. 2018)
Early-Burdigalian
Channels
Afiq Canyon
Levant
Basin
N-S
trending
channels
NW-trending
delivery system
(Hordos)
Early Miocene
Incision
Temash - Bardawill
Trend
Offshore
Canyon
Hannaha-1
well
32°
Judea Hills
Uplift
Middle Hazeva
(Rotem)
Middle Miocene Shoreline
re-activation
of the
SNZS
EGYPT
Folding
onshore
Sinai
Proto
Nile
River
Initiation
of
Dead-Sea
transform
(~18 Ma)
50 km
Themed Fault
Suez
Rifting
32°
34°
B
Dead-Sea
Fault
Hazeva
Oligocene Truncation
Surface
Red Sea
Rifting
Judea Hills
Uplift
Irbid Rift
Faulting
Nile
Sinai
Folding
Hordos
Formation
N
Initial
Offshore Thinning
Eocene
Marls
Early Burdigalian (21.2 - 17.54 Ma)
not to scale

1053 Figure 15

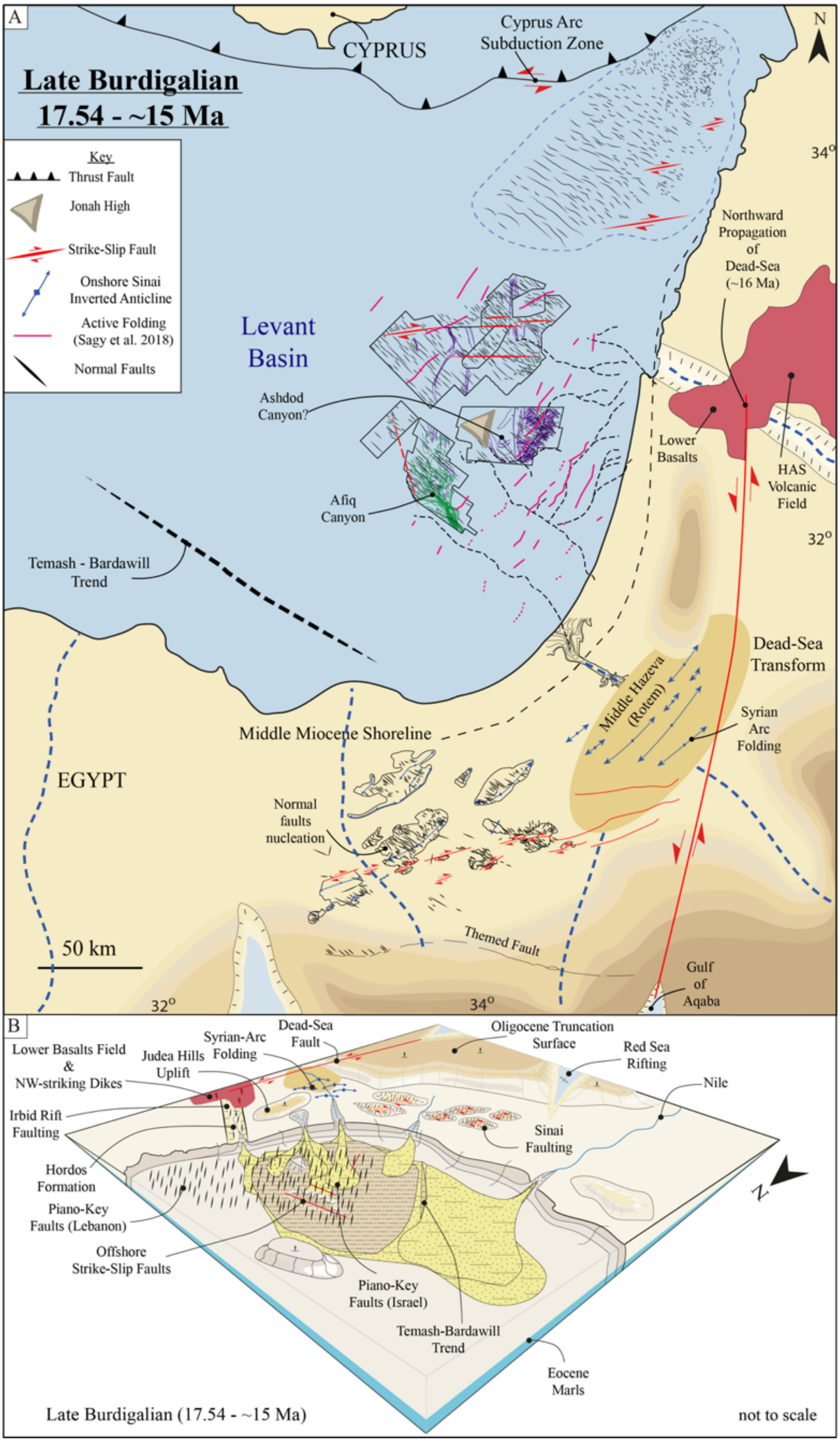

1054
1055

1056 Figure 16

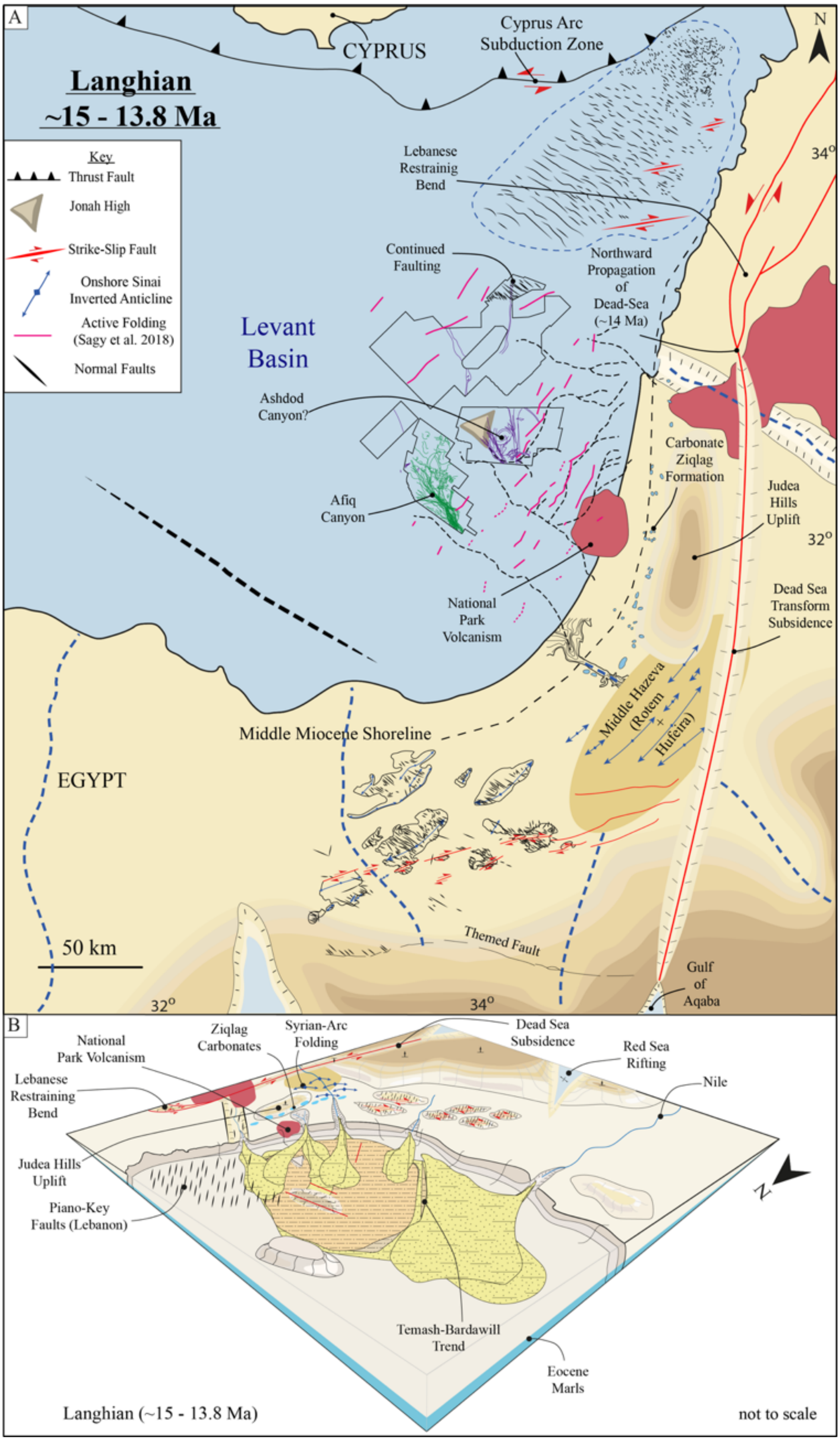

1057

1058

Figure 17

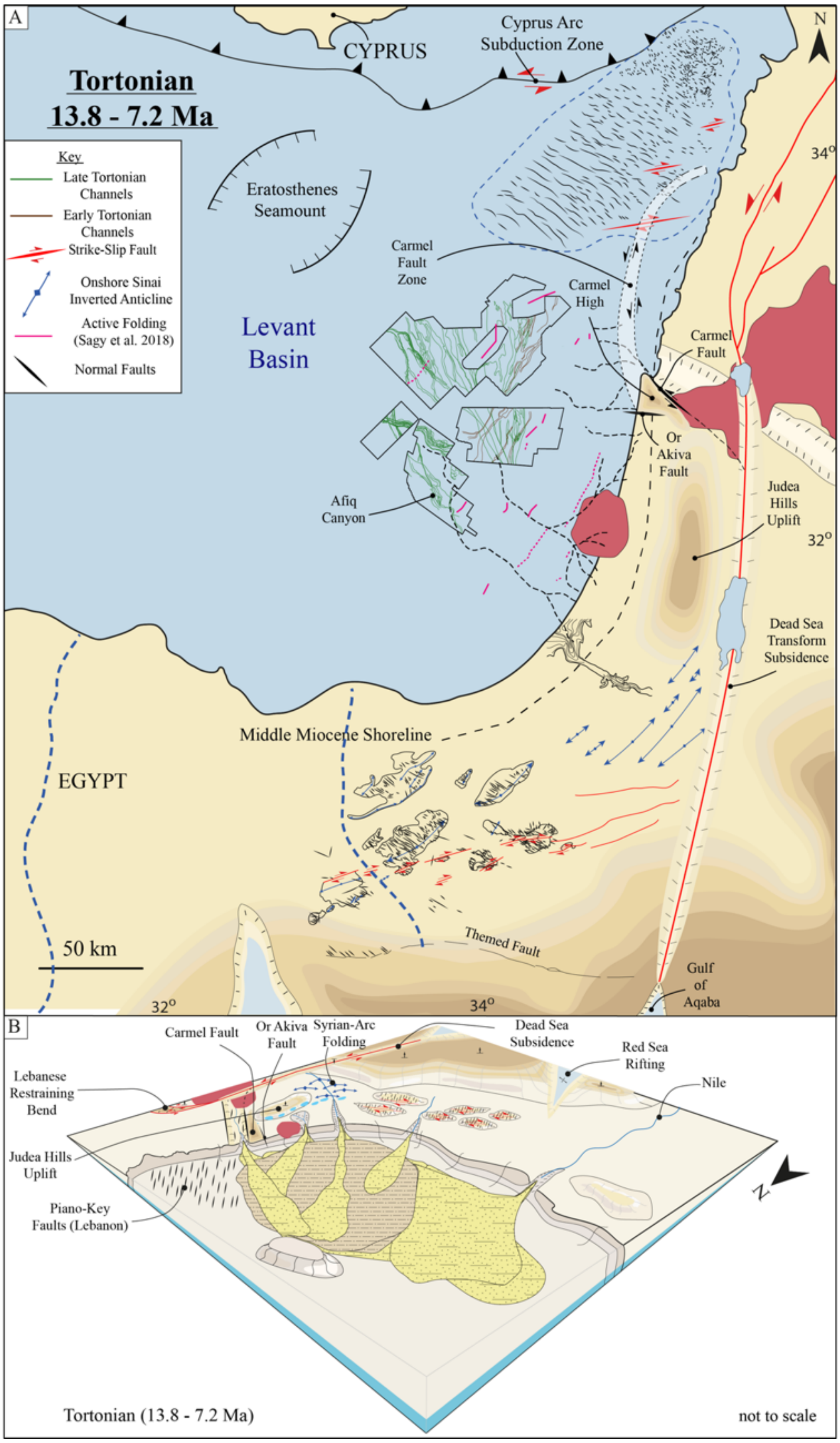

A
Tortonian
13.8 - 7.2 Ma
CYPRUS
Cyprus Arc
Subduction Zone
N
Key
Late Tortonian Channels
Early Tortonian Channels
Strike-Slip Fault
Onshore Sinai Inverted Anticline
Active Folding (Sagy et al. 2018)
Normal Faults
Eratosthenes Seamount
Levant Basin
Carmel Fault Zone
Carmel High
Carmel Fault
Or Akiva Fault
Afiq Canyon
Judea Hills Uplift
Dead Sea Transform Subsidence
34°
32°
Middle Miocene Shoreline
EGYPT
50 km
Themed Fault
Gulf of Aqaba
32°
34°
B
Carmel Fault
Or Akiva Fault
Syrian-Arc Folding
Dead Sea Subsidence
Red Sea Rifting
Nile
Lebanese Restraining Bend
Judea Hills Uplift
Piano-Key Faults (Lebanon)
N
Tortonian (13.8 - 7.2 Ma)
not to scale